

UC Santa Cruz

UC Santa Cruz Electronic Theses and Dissertations

Title

Mechanism of anti-tumor compounds that inhibit the spliceosome

Permalink

<https://escholarship.org/uc/item/1h62r0t9>

Author

Lopez, Adriana Gamboa

Publication Date

2021

Copyright Information

This work is made available under the terms of a Creative Commons Attribution License, available at <https://creativecommons.org/licenses/by/4.0/>

Peer reviewed|Thesis/dissertation

UNIVERSITY OF CALIFORNIA
SANTA CRUZ

**Mechanism of anti-tumor compounds
that inhibit the spliceosome**

Doctor of Philosophy

In Molecular, Cellular and Developmental Biology

By

Adriana Gamboa Lopez

March 2021

The dissertation of Adriana Gamboa
Lopez is approved by:

Professor Melissa S. Jurica, Chair

Professor Manuel Ares, Jr.

Professor Charles Query, Albert Einstein
College of Medicine

Quentin Williams
Acting Vice Provost and Dean of Graduate Studies

Copyright © by
Adriana Gamboa Lopez
2021

Table of contents

1. List of figures.....	iv
2. List of supplementary figures.....	vi
Abstract.....	vi
Acknowledgments.....	viii
Chapter 1: Pre-mRNA splicing	
1.1 Gene Expression.....	1
1.2 Function of the Spliceosome.....	1
1.3 Current State of the Splicing Field.....	3
1.4 U2 snRNP in early spliceosome assembly.....	5
1.5 SF3B1 guider of the U2 snRNP.....	6
1.6 Mutations in SF3B1 produce aberrant transcripts.....	6
1.7 Diseases associated with SF3B1 mutations.....	7
1.8 Drugs that target SF3B1 help us learn about splicing and cancer.....	8
1.9 Contribution to the Dissertation.....	10
Chapter 2: Small drug molecules: tools to study the spliceosome	
2.1 Discovery of Small drug molecules that target SF3B.....	12
2.2 Structural evidence SF3B1 inhibitors bind to Branchpoint Adenosine pocket.....	14
2.3 What do drugs do in cells and their chemical relevance.....	15
2.4 Overview of Spliceostatin A.....	18
2.5 Overview of Pladienolide B.....	19
2.6 Overview of herboxidiene.....	20

2.7 Challenges when creating SF3B1 inhibitors and contribution to the dissertation.....	23
---	----

Chapter 3: Herboxidiene features that mediate conformation-dependent SF3B1 interactions to inhibit splicing

3.1 Abstract.....	25
3.2 Introduction.....	26
3.3 Results and discussion	29
3.4 Conclusion.....	44
3.5 Materials and methods.....	46
3.6 Supplementary Information.....	48

Chapter 4: The effects of SF3B1 inhibitor on the U2 snRNP

4.1 Introduction.....	52
4.2 Results and Discussion	52
4.3 Conclusion.....	57
4.4 Materials and Methods	59

Chapter 1

Figure 1-1 Eukaryotic gene expression.....	2
Figure 1-2 Overview of splicing cycle and two-step chemistry.....	4
Figure 1-3 Pre-mRNA	5
Figure 1-4 SF3B1 mutations lead to misregulation in splicing.....	7
Figure 1-5 SF3B1 mutations associated with disease.....	8
Figure 1-6 Cryo-EM structure of Bact spliceosome.....	10

Chapter 2

Figure 2-1 Chemical structures of active compounds and inactive analogs.....	13
Figure 2-2 Inactive compounds can be used interchangeably to rescue splicing.....	22
Figure 2-3 Crystal structure of SF3B1.....	16
Figure 2-4 HB tunneled between SF3B1 and PHF5A.....	16
Figure 2-5 SSA and derivates.....	19
Figure 2-6 PB and derivates.....	21
Figure 2-7 HB and derivates.....	22
Figure 2-8: New derivatives of herboxidiene inhibit spliceosome assembly.....	23

Chapter 3

Figure 3-1: Temperature and ATP influences inhibitor access to SF3B.....	26
Figure 3-2 Order of addition affects competition between SF3B inhibitors and an inactive herboxidiene analog.	31
Figure 3-3 Temperature affects competition between SF3B inhibitors and inactive analogs.	33
Figure 3-4 Temperature-dependent modulation of SF3B inhibition is independent of ATP.....	35
Figure 3-5 SF3B inhibitors exchange more slowly than inactive analogs.....	39
Figure 3-6 Structure activity relationships for herboxidiene activity and SF3B interaction.....	42
Figure 3-7 Model of early spliceosome assembly and SF3B inhibition.....	44

Chapter 4

Figure 4-1 PB promotes 17S U2 snRNP.....	54
Figure 4-2 PB has no effect on SF3B3 migration.....	55

Figure 4-3 PB has no effect on SNRPB2 migration.....56

Figure 4-4 Proteins and U2 snRNA in Native Gels.....58

List of supplementary Figures

Suppl. Figure 3-1 Chemical Structure of SF3B inhibitor analogs used in this study.....48

Suppl. Figure 3-2 Order of addition affects competition between SF3B inhibitors and inactive PB and SSA analogs.....49

Suppl. Figure 3-3 Temperature affects competition with iSSA and iPB but not inactive and active compound controls.....50

Suppl. Figure 3-4 Temperature dependent inhibition of splicing depends on order of addition of excess inactive competitor..... 51

Suppl. Figure 3-5 Pre-mRNA sequence of substrate used in splicing for this study.....51

Bibliography.....62

Abstract

Adriana Gamboa Lopez

Mechanism of anti-tumor compounds that inhibit the spliceosome

The spliceosome is a dynamic ribonucleo-protein complex that is in charge of removing introns from pre-mRNA. Five small nuclear ribonucleic proteins (snRNPs) (U1, U2, U4, U5, U6) build the spliceosome, and each contain their own special RNA. In particular, U2 snRNP is unique, in that it guides the spliceosome to the correct branch point sequence. SF3B1 is the largest and keystone protein of U2 snRNP. Mutations in SF3B1 have been associated with misregulation in splicing and disease such as cancer. Spliceostatin A, Pladienolide B and herboxidiene are small drug molecules that target SF3B1. They are used as tools to help study the importance of SF3B1 and initiation of splicing assembly. However, the mechanism of action of these molecules is not known. More studies need to research how these drugs bind and inhibit. I used *in vitro* order of addition splicing assays, and studied SF3B1 in different conditions: temperature, time, and competition assay. My findings clearly demonstrate that temperature affects competition between active and inactive compounds. Time course experiments clearly imply that SF3B inhibitors exchange more slowly than inactive analogs. Lastly, we show positions C1 and C6 of herboxidiene are important for binding and inhibiting SF3B1 in the binding pocket. We also model drug-protein interaction. Our work will help elucidate how SF3B1 selects the correct branch point sequence and give medicinal chemists new insights to make small molecule drugs more potent.

Dedication and Acknowledgements

I want to thank my God, creator of the universe, for always being with me and giving the opportunity to learn about his creation. If it was not for science and nature, I would not believe in a God.

Romans 1:20

For his invisible attributes, namely, his eternal power and divine nature, have been clearly perceived, ever since the creation of the world, in the things that have been made. So, they are without excuse.

I thank Bernarda De Casas, Elpidia Gamboa, and Monica Lopez for being strong women who taught me faith, love, strength and compassion. My father, Pablo Lopez, who taught me to work hard and sacrifice. My siblings Pablo, Brenda, Abraham and Monica Lopez for all of their love and support. My husband to be, Rob Hillebrecht, for taking care of me and making sure that I get my work done. Dr. Melissa Jurica for teaching me all that I know. Jurica lab for teaching me how to splice and being supportive of my presentations. Oakes College for allowing me to mentor students and providing me with a family. Campbell Church of Christ members for loving me and adopting me these past five years. STEM Diversity, Yulianna Ortega, for being there for me whenever I need to shed some tears.









Chapter 3 is a modified version of the following publication:

Gamboa Lopez A, Allu SR, Mendez P, Chandrashekar Reddy G, Maul-Newby HM, Ghosh AK, Jurica MS. Herboxidiene Features That Mediate Conformation-Dependent SF3B1 Interactions to Inhibit Splicing. ACS Chem Biol. 2021 Feb 22. doi: 10.1021/acscchembio.0c00965. Epub ahead of print. PMID: 33617218.

Approval to use the publications as part of the dissertation was obtained from the American Chemical Society Chemical Biology.

Chapter 4

I would like to give credit to Matt Modena and Andrew MacRae who initiated the western/native protocol that is independent of this project. I want to also give credit to Hannah Maul-Newby for optimizing the western/native protocol and getting it to work.

Chapter 1: Introduction to Pre-mRNA splicing

1.1 Gene Expression

Eukaryotic gene expression is the process in which the cell self-regulates what proteins are needed to function and survive. Shown in Figure 1-1, the information is transferred in three main steps: transcription, RNA processing and translation. In transcription, a single-stranded DNA is transcribed to pre-mRNA. Splicing is co-transcriptional, where the pre-mRNA is capped, undergoes splicing, where selected intron sequences are removed, and leftover exons are ligated. Afterwards the mRNA is 3' poly-adenylated. The mRNA is exported out of the nucleus into the cytoplasm where it is then translated into a protein by the ribosome. How the cell regulates each of these steps is still a mystery. My thesis will focus on splicing, which is regulated by the spliceosome, a dynamic ribonucleic-protein complex.

1.2 Function of the spliceosome

The spliceosome is a biological scissor that removes selected introns from pre-mRNA. The spliceosome is composed of five small nuclear U-rich RNAs (snRNAs) and over 150 proteins. The main components of the spliceosome are five small nuclear ribonucleoproteins (snRNPs) which consist of: U1, U2, U4, U5, U6 snRNP that are individually assembled with their protein components and snRNA. The spliceosome is very dynamic as it is constantly rearranging with intermediate steps involving protein-protein, RNA-RNA, protein-RNA interactions.

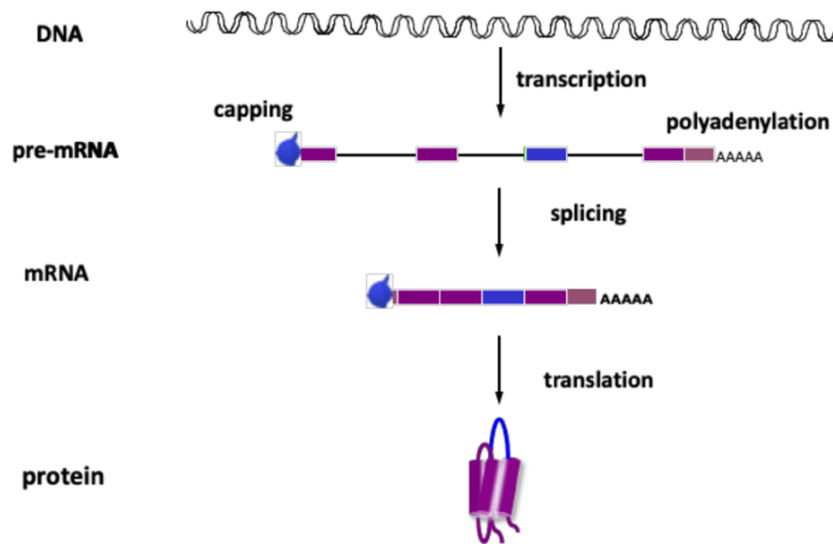


Figure 1-1: Eukaryotic gene expression.

DNA is transcribed to pre-mRNA, 5' capped, spliced and a 3' poly(A) tail is added. The mRNA is translated into protein by the ribosome. Exons are represented by blue and purple boxes and introns are represented by black lines in the pre-mRNA. (Created by Dr. Melissa S. Jurica.)

The stepwise interactions between the spliceosome and pre-mRNA assembly occur when the U1 snRNP recognizes the 5' splice site to form Complex E (Figure 1-2.A). Afterwards, U2 snRNP binds to the branch point sequence (BPS) to form the Complex A or pre-spliceosome. The tri-snRNP (U4/5/6) then joins the Complex A to generate Complex B (Pre-catalytic spliceosome). After Complex B rearrangements, U1 and U4 are released, forming B^{act} (activated) complex, leading to the B* (catalytically activated) complex. This yields the C complex, which is catalyzed as the first step of chemistry. After splicing, the spliceosome is disassociated, and the cycle is repeated.

Splicing involves two trans-esterification reactions steps to successfully create a mature RNA (Figure 1-2. B). In the first step, the adenosine on the intron attacks the 5' splice site releasing the 5' exon and intron bound to the 3' exon. In the second trans-

esterification step, the 5' exon attacks the 3' splice site to produce mature mRNA and the lariat intron.

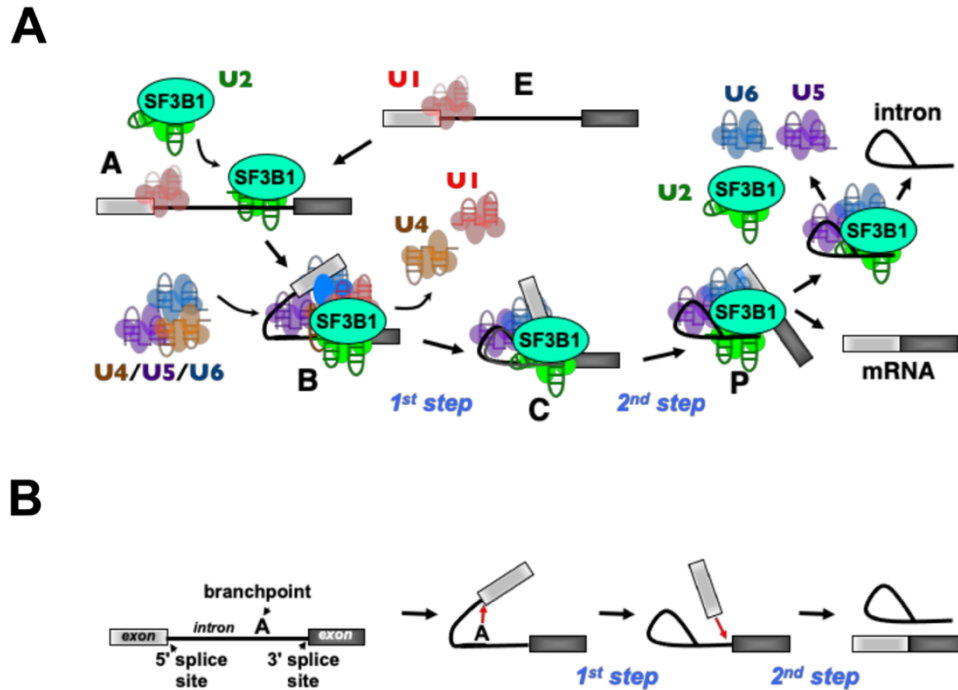


Figure 1-2: Overview of splicing cycle and two steps splicing of chemistry.

A) Formation of the spliceosome on the pre-mRNA. U snRNPs assemble in a stepwise manner. SF3B1 is involved throughout splicing **B)** Two transesterification steps allow for splicing products. In the first step, 5' exon and lariat-3' exon are formed. In the second step of chemistry, both exons are ligated to form mRNA, and free lariat is formed. (Created by Dr. Melissa S. Jurica)

1.3 Current state of the splicing field

We are currently in a boom of a structural era, where decades of biochemical and yeast genetic research tethered with new cryo-EM and crystallography provide the foundation to delve more into the molecular mechanisms of spliceosome assembly (Wilkinson et al., 2020). The splicing field has been able to capture parts of the

spliceosome in action. For example, B^{act} , the step in which the spliceosome is activated, but not catalytically primed, was captured using cryo-EM in both yeast and human spliceosomes (Wilkinson et al., 2020; Kataoka, 2017). Both of these structures demonstrate protein-protein and RNA-RNA interactions between U2 and U5 snRNP, U6 snRNA and pre-mRNA. As exciting as it is understanding how the spliceosome assembles, we still do not know all the components that are involved and how they come together. One limitation with using cryo-EM is the limited resolution, which ranges from 3-10 Angstroms. The dynamic nature of the spliceosome with its many transition states and ATP-dependent proteins rapidly coming on and off, makes it difficult to capture a single conformation. An alternative to using cryo-EM is chemical probing to document conformational changes. The Jurica Lab developed a protocol to measure changes in lysine accessibility in RNPs (MacRae et al., 2019). With this technology we can characterize complexes that are found in small quantities, which is ideal since some complexes are less abundant than others.

In addition to not fully understanding all of the components of the spliceosome and experimental limitations due to its dynamic nature, we add the complexity of the pre-mRNA. Although seemingly simple, each sequence of the pre-mRNA serves to orchestrate the spliceosome. The pre-mRNA contains six special sequences: exons, introns, consensus sequences containing the branch point adenosine (BPS), 5' splice site (5'SS), 3' splice site (3'SS) and polypyrimidine tract (PPT) (Kataoka, 2017), (Figure 1-3). Each of the sequences are separated within a certain proximity from one another. The BPS is 18-40 nucleotides upstream from the 3' SS and is then followed

by the PPT (Kataoka, 2017). The splicing field is still trying to address how the pre-mRNA serves as a landing pad for the spliceosome. With the many spliceosome structures, biochemical assays and genetic screens that we have, much research is needed to fully study the spliceosome at the molecular level. Later on, I will discuss a tool that has not only opened the doors for the splicing field to gather molecular clues as to how the spliceosome works, but that also helps us understand how it recognizes these simple yet essential pre-mRNA sequences.

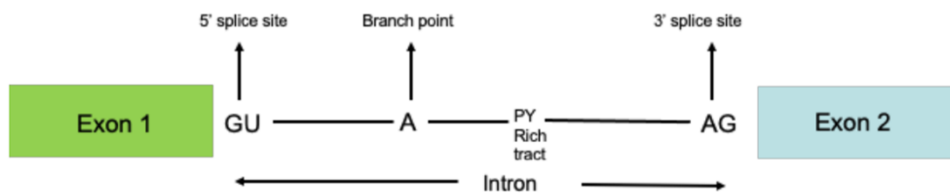


Figure 1-3: Pre-mRNA.

Pre-mRNA consists of exons, introns, 5' splice site, 3' splice site, branch point adenosine and polypyrimidine tract.

1.4 U2 snRNP in early spliceosome assembly

One key component in the spliceosome is the U2 snRNP, which is involved throughout the splicing cycle. It is in charge of selecting the correct BPS to form Complex A. There are two forms of U2 snRNP, 17S U2 snRNP which joins the spliceosome and 12S U2 snRNP that is released after splicing. The 12S U2 snRNP, is composed of the U2 snRNA and core proteins. The 17S U2 snRNP, is composed of three multiprotein families that assemble in the following order 12S U2 snRNP + SF3B → 15S U2 snRNP + SF3A → 17S U2 snRNP. The U2 snRNP has been studied

since the early 1990s by the Kramer, Lührmann and Reed lab groups and yet it is not fully understood how the U2 snRNP selects the canonical branch point sequence (Brosi et al., 1993; Gozani et al., 1998; Kramer et al., 1999; Chiara et al., 1996).

1.5 SF3B1 guides the U2 snRNP to the correct branch point sequence

SF3B1 is the largest component that belongs to the SF3B multi-complex protein family with 22 heat-repeats and has been shown to help guide the U2 snRNP to the correct sequence (Gozani et al., 1998). What is most fascinating about this protein is that cryo-EM and crystallography structures have shown that SF3B1 is in either an “open” or a “closed” conformation, forming a clamp. The current model for SF3B1 is that it guides the U2 snRNP to the pre-mRNA where it serves to pinch the BPS to the U2 snRNA. Afterwards, U2 snRNA undergoes many rearrangements during splicing, and what controls U2 snRNA rearrangement is unknown. DDX46 (Prp5 in yeast), an ATP-dependent helicase, is needed to form a pre-spliceosome (O'Day et al., 1996). Excitingly, a recent paper by the Lührmann group revealed that ATP-dependent helicase DDX46 and HTATSF1 hold the U2 snRNP in the “open” conformation while also holding the U2 snRNA in the BSL form (Zhang et al., 2020).

1.6 Mutations in SF3B1 lead to aberrant transcripts

A single intron contains many BPS (YUNAY) and 3'SS (YnNCAG) sequences, and selection of the incorrect BPS will produce an aberrant transcript which will result in an aberrant protein or will be degraded through nonsense-mediated decay. Selection of the noncanonical BPS can induce selection of the wrong 3'SS (Darman et al., 2015). Mutations in SF3B1 have been associated with diseases such as cancer where mutations

occur in heat repeats 4-12, and lead to changes in BPS selection. Figure 1-4 illustrates the impact of SF3B1 mutations in splicing (Zhou et al., 2020).

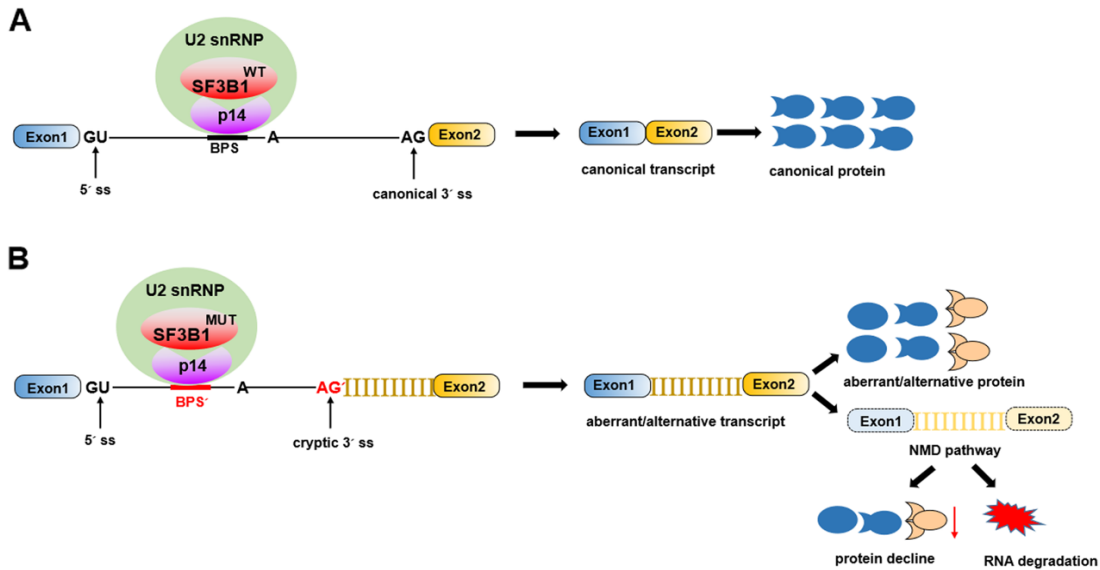


Figure 1-4: SF3B1 mutations lead to misregulation in splicing.

A) Wild-type SF3B1 recognizes both the canonical branch point sequence and 3' splice site leading to canonical protein production. **B)** Mutated SF3B1 selects an upstream branch point sequence leading to selection of cryptic 3' SS. An aberrant protein is produced or nonsense mediated decay results in RNA degradation (Zhou et al., 2020).
© Springer Nature

1.7 Diseases associated with SF3B1 mutations

Mutations in genes encoding splicing factors have been found in myelodysplastic syndromes (MDS), acute myeloid leukemia (AML) patients and solid tumors such as breast and pancreatic cancers (Schmidt et al., 2011; Yoshida and Ogawa, 2014; Maguire et al., 2015; Papaemmanuil et al., 2011). Certain SF3B1 mutations such as K700E are more common in ER-positive types of breast cancer (Maguire et al., 2015). In MDS patients, specific mutations in SF3B1 were associated

with ring sideroblast phenotypes (Cazzola et al., 2013). SF3B1 mutations in uveal melanoma were associated with alternative splicing of the 3' end of transcripts (Furney et al., 2013). The biological relevance of SF3B1 is important to study for human health. The mechanism of action of what allows for certain SF3B1 mutations to be associated with specific disease types is not very well understood, Figure 1-5 (Zhou et al., 2020).

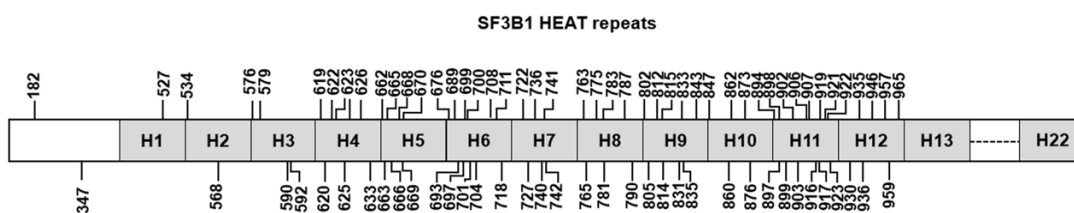


Figure 1-5: SF3B1 mutations associated with disease.

Heat repeats 4-12 contain the most mutations in the SF3B1 gene (Zhou et al., 2020). © Springer Nature

1.8 Drugs that target SF3B1 help us learn about splicing and cancer

Spliceostatin A (SSA), Pladienolide B (PB) and herboxidiene B (HB) represent three small-molecule families with complex structures that target SF3B (Yokoi et al., 2011). All of these drugs have been extracted from bacteria and contain antitumor properties. PB has been found to inhibit growth in 37 cancer cell lines which include prostate and breast cancer cells. (Mizui et al., 2004). To investigate what bound to SSA, an experiment in which biotinylated SSA was used to pull down proteins associated with the drug identified SF3B compounds. Furthermore, LC-MS/MS analysis revealed that those proteins were components of the SF3B multi-protein family (Kaida et al., 2007). Western blotting using SF3B antibodies gave additional evidence that these proteins were indeed from SF3B. They are referred as “SF3B1 inhibitors” since after

one wash with SDS-containing buffer the only protein bound to biotinylated SSA was SF3B1.

One large gap in the field is how do these small-drug molecules inhibit splicing? Currently, it is known that all three inhibitors stall splicing at Complex A, but when HeLa nuclear extract with PB was challenged by heparin, Complex A was unstable (Effenberger et al., 2016b). SF3B1 structure model PB embedded near residues of the BPS-binding pocket, these residues are consistent with residues that confer resistance or sensitivity to PB (Cretu et al., 2018; Finci et al., 2018). Figure 1-6 demonstrates how SF3B1 clamps U2 snRNA and pre-mRNA (Yan et al., 2016). Expanded upon in Chapter 2, all structures have different chemical structures and IC50s (the concentration needed to reduce *in vitro* splicing by half), they all target the same binding site (Effenberger et al., 2016b). It is not known at what splicing stage inhibitors binds to SF3B1 or if drugs join the U2 snRNP, SF3B or SF3B1 first? My research will help in understanding how these small-drug molecules interact with SF3B1 and how we can use that information to modify chemical features to use them as chemotherapeutics. In addition, we will learn how mutations in SF3B1 lead to mis-regulation in splicing, which leads to all kinds of diseases.

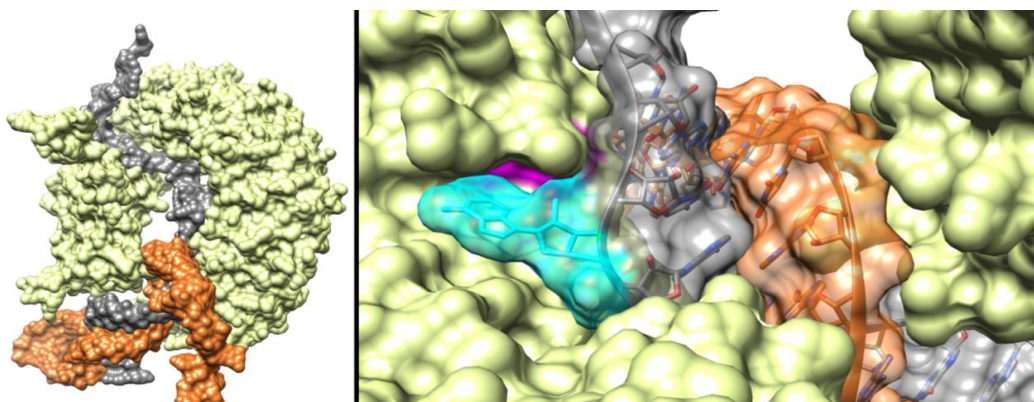


Figure 1-6: Cryo-EM structure of B^{act} spliceosome.

A) SF3B1 (yellow) in a closed conformation clamping U2 snRNA (orange) and pre-mRNA (gray). **B)** Close-up of branch region/U2 snRNA base pairs with bulged adenosine (cyan) near the SF3B1 inhibitor resistance mutations (magenta). Adapted from Yan et al. *Science* 2016 by Dr. Melissa S. Jurica.

1.9 Contribution to the dissertation

Excitingly, we have a snapshot of different SF3B1 conformations and a model of how SF3B1 guides the U2 snRNP to the correct BPS. However, we do not know at what stages each SF3B1 conformation occurs or what controls for conformational changes. A current model suggests that inhibitors hold SF3B1 in an open conformation, but it is still not known what chemical features allow for inhibition and binding. The goal of my dissertation is to understand the following: 1) The role of SF3B1 in early spliceosome assembly 2) Expand our knowledge of inhibitors to use as tools to study SF3B1 3) Understand how SF3B1 inhibitors affect the U2 snRNP in terms of protein and RNA composition. In Chapter 2, I discuss small drug molecules that target SF3B, give an overview of their structure, clinical relevance to cancer and implications to the splicing field. In Chapter 3, I will present findings that support different SF3B1 conformations in early spliceosome assembly and chemical features that are important

for inhibition. I delve more into understanding herboxidiene, as it is simpler relative to PB because of the smaller ring. We will identify chemical features that tolerate changes and those that are required for inhibition. Lastly, in Chapter 4, I will present preliminary data exploring how SF3B inhibitors affect U2 snRNP. My thesis will help the splicing field learn more about the mechanism of how SF3B1 guides the U2 snRNP to the correct BPS.

Chapter 2: Discovery of small drug molecules that target SF3B

2.1 Biochemical evidence inhibitors target SF3B

SF3B1 inhibitors (PB, SSA, HB) have complex chemical structures and target SF3B. They require varying concentration to inhibit splicing and it is not known what allows them to have different potencies. To further investigate how small-drug molecules target SF3B complex, the Jurica and Ghosh Lab investigated the structure-activity relationships of the compounds and identified inactive analogs (Figure 2-1) (Effenberger et al., 2016b). Essentially, inactive analogs have similar chemical structures as their active parent drugs but have extra or removed chemical features preventing them from inhibiting, but still bind to SF3B. Inactive analogs are used as competitors. In a splicing *in vitro* assay, adding inactive compound allowed for splicing. To investigate if compounds were inactive because they did not interact with SF3B1 or because they do not interfere with SF3B1 function; a competition *in vitro* assay was developed in which active and varying concentrations of inactive compounds were added simultaneously. Results indicate that splicing can be rescued when higher concentrations of inactive compounds were added along with the active compounds (Figure 2-2). Thus, the inactive compounds serve as competitors of SF3B1 inhibitors.

Effenberger et al. wanted to investigate if all three active compounds bind the same SF3B1 site. They used the same competition assay in which they added active drug with varying concentrations of inactive compounds. The only difference in this assay was that the inactive compound was structurally different from the parent active compound. Results indicate inactive compounds can outcompete other active

compounds that were structurally different. These data suggest that all active compounds and their inactive competitors bind the same SF3B1 site. The next step to understanding how SF3B1 functions and what the drugs target is through structural studies of drug/protein interactions. In the next section, I will review SF3B1 structures from different splicing steps observed in yeast and human cells.

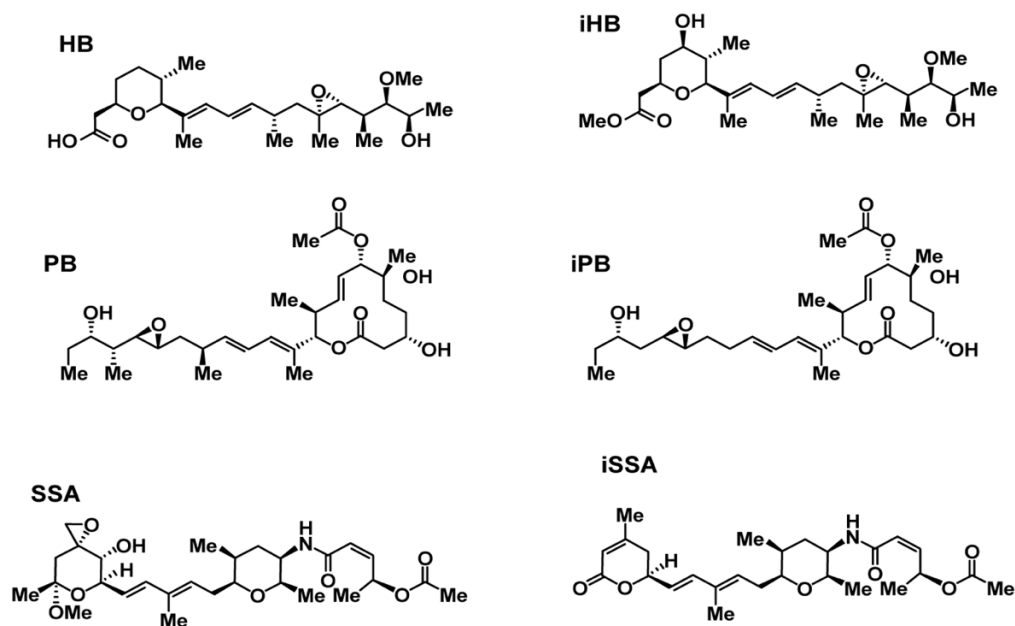


Figure 2-1: Chemical structures of active compounds and inactive analogs.

Left column active compounds top to bottom. HB: herboxidiene, PB: Pladienolide B and SSA: Spliceostatin A. Right column inactive compounds top to bottom. inactive HB, inactive PB and inactive SSA (Effenberger et al., 2016b).

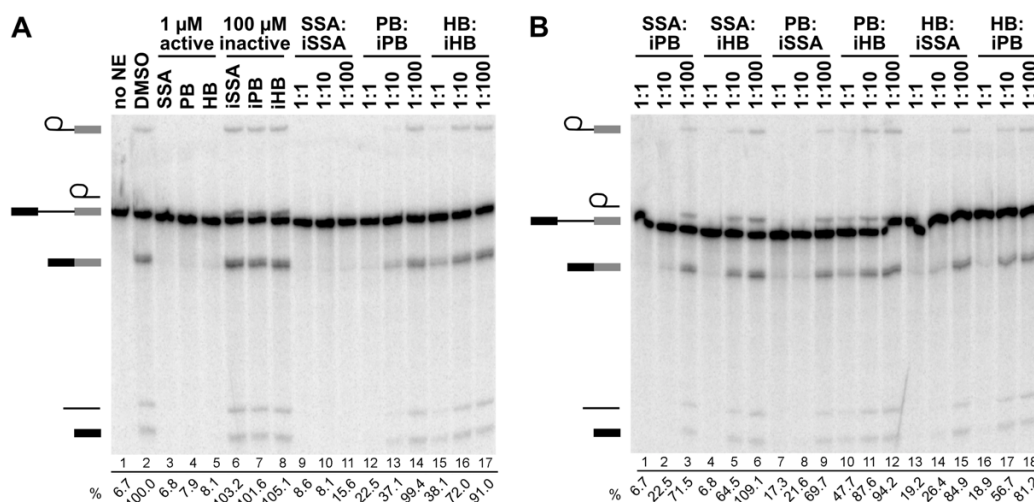


Figure 2-2: Inactive compounds can be used interchangeably to rescue splicing.

Representative denaturing gels of *in vitro* splicing. **A)** Competition phases were done by adding SSA (1 μ M), PB (1 μ M), or HB (1 μ M), simultaneously with iSSA, iPB or iHB at different concentrations (1, 10, 100 μ M). **B)** Same as A except an inactive compound was added that did not belong to the same family of the active compound. (Effenberger et al. 2016).

2.2 Structural evidence that SF3B1 inhibitors bind to the Branch Point Adenosine pocket

The first SF3B1 human crystal structure was isolated along with SF3B proteins (Cretu et al., 2016). When the structure was overlaid with yeast structure from the B^{act} of yeast, there was a clear distinction of “opened” and “closed” SF3B1 protein (Yan et al., 2016; Finci et al., 2018; Cretu et al., 2018). Figure 2-3 illustrates the “opened” and “closed” states of SF3B1.

Cryo-EM and crystallography structures modeled SF3B1 inhibitors binding to SF3B. In a cryo-EM structure, E7107, a PB derivative, was shown to bind at the interface of SF3B1 and PHF5A. Compound binding did not have a conformational

impact on SF3B1, SF3B3, SF3B5 and PHF5A. In fact, the conformation of these four proteins were similar to that of the human crystal structure of SF3B.

Months after the publication of the E7107 bound to SF3B1 using cryo-EM, the Pena lab reported a structure of PB bound to SF3B demonstrating how PB binds close to the branch sequence adenosine pocket (Cretu et al., 2018). PB is wedged between SF3B1 heat repeats 15, 16, 17 and PHF5A, preventing SF3B1 from forming a “closed” state. The consequences of leaving SF3B1 in an “open” state is that branch helix may not be fully docked on SF3B, which could explain why the drugs stall at an unstable Complex A (Folco et al., 2011; Effenberger et al., 2016b). One common feature that all of these drug’s hold is a diene group in the center of the drugs. The diene group of PB is sandwiched in the middle of a tunnel like feature formed by SF3B1 and PHF5A (Figure 2-4) (Lopez, A.G., et. al. 2021). This finding is consistent with an earlier model demonstrating that SF3B1 inhibitors bind to a pocket near SF3B multi-complex protein (Teng et al., 2017). We have biochemical and structural data showing how SF3B1 inhibitors affect splicing, but what do they do in cells?

2.3 What do drugs do in cells and what is their medical relevance?

There are many variables that can be measured in cells: cell cycle effects, growth rates, alterations in splicing. PB was shown to inhibit growth of six drug-resistant cells lines. WiDr and DLD1 human colorectal cancer cells were used to develop PB resistant cells lines, but more molecular evidence was needed to understand inhibition (Mizui et al., 2004). Using mRNA-Seq differential analysis of cancer cells, mutations in SF3B1 were discovered (Yokoi et al., 2011). A similar study was

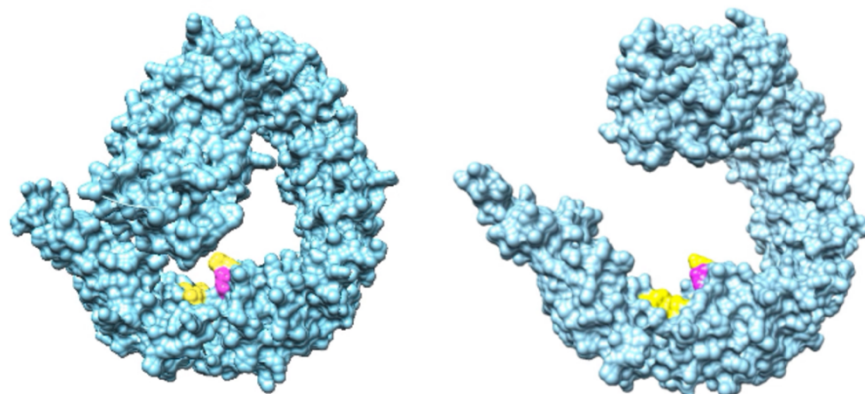


Figure 2-3: Crystal structure of SF3B1.

SF3B1 is highlighted in blue. Yellow represent areas resistant to drugs and pink represents compound target. **A)** SF3B1 closed state **B)** SF3B1 open state. Adapted from Cretu 2016. Created by Dr. Melissa S. Jurica.

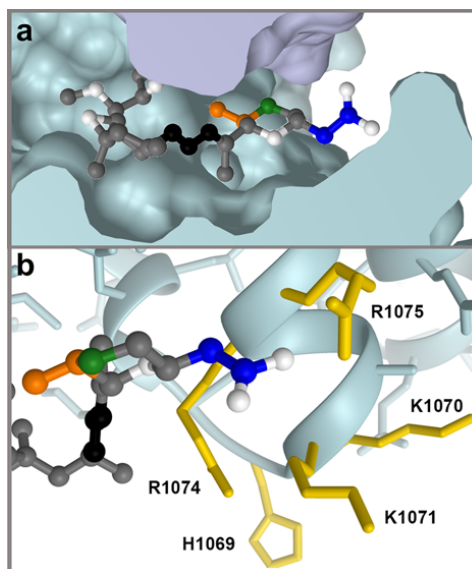


Figure 2-4: HB tunneled between PHF5A and SF3B1.

A) Model of herboxidiene bound to SF3B inhibitor channel between SF3B (teal) and PHF5A (purple). **B)** Mutations of labeled residues in yellow confer resistance to Pladienolide B or herboxidiene. (Lopez, A.G., et. al. 2021).

conducted in which E7107 and herboxidiene were used in HCT116 human colon cancer cell lines to investigate if cells would evolve mutations that confer resistance to drugs. New resistance mutations were found in PHF5A (Teng et al., 2017). Growth inhibition profiling of resistant clones of SF3B1 (R1074H, V1078I and V1078A) and PHF5A (Y36C) were shown to confer resistance to SF3B1 inhibitors. Not only can cells form mutations with inhibitors, but also affect structures in the nucleus. SF3B1 inhibitors convert nuclear speckles to mega speckles, which are cell bodies containing snRNPs, SR proteins and transcription factors. Accumulation of unspliced transcripts were found in nuclear speckles when splicing was inhibited (Effenberger et al., 2014; Carvalho et al., 2017; Idowu et al., 2015). PB was shown to induce cell cycle and apoptosis in human cervical carcinoma cells and inhibited SF3B1 expression at higher drug concentrations (Zhang et al., 2019). It is not known if nuclear speckles are independent of cell arrest or if they are related. We also do not know if there is a signaling cascade connecting all of these pathways.

Another question is how do SF3B1 inhibitors affect at the transcriptome level. RNAseq data show that only some genes show strong splicing changes and not all changes are consistent. Exon skipping was observed following SF3B1 inhibition (Wu et al., 2018). It is very unclear how changes in alternative splicing occur in the presence of drugs. Vigevani et al. demonstrated drug structure has an effect on exon skipping and intron retention. For example, SSA had a higher intron retention than Sudemycin (Vigevani et al., 2017). It is important to study the molecular mechanism of these drugs

to better understand off-target effects and how to target cancer cells. One concern about using inhibitors is how do we make sure they don't kill cells that are not cancerous? One study demonstrated that exposing PB to normal skin cells leads to apoptosis through the p53 pathway (Hepburn et al., 2018). Therefore, it is in our interest to continue to pursue SF3B1 inhibitors as chemotherapeutics (Lee et al., 2016).

2.4 Overview of SSA

SSA derivatives (FR901463, FR901464 and FR901465) were isolated from the culture of bacterium *Pseudomonas sp.* N. 2663 where FR901464 was found to be the most promising for anti-tumor effects (Nakajima et al., 1996b; Nakajima et al., 1996a). Since then, SSA has been studied at the molecular level in *in vivo* studies (Thompson et al., 2001; Ghosh et al., 2014a; Roybal and Jurica, 2010). Studies using SSA have demonstrated that it causes apoptosis in chronic lymphocytic leukemia (Larrayoz et al., 2015). Yoshimoto et al. investigated the global effect of SSA on splicing and determined SSA caused intron retention and short transcripts leak into the cytoplasm (Yoshimoto et al., 2017). It is not known what allows for intron retention in SSA as other SF3B1 inhibitors do not have the same effect. One recent derivative of SSA (1,2-deoxy-pyranose derivative) inhibited androgen receptor splice variant 7 (AR-V7) at 3.3nM, which is much more potent than SSA at IC₅₀70nM, passed an *in vivo* toxicity evaluation using wild-type mice (Yoshikawa et al., 2020; Effenberger et al., 2016b). SSA is the most potent of SF3B1 inhibitors. SSA has been evaluated to be a tumor growth suppressor, but one of the challenges of SSA is synthesizing and designing chemical features to the complex structure (Figure 2-5).

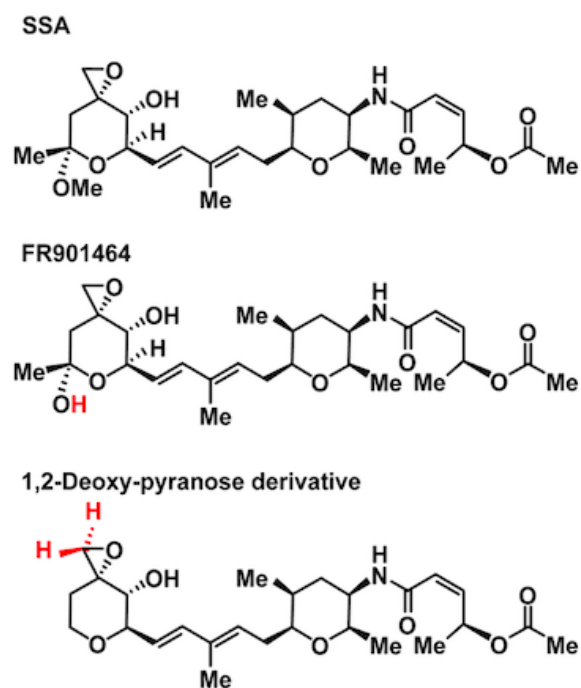


Figure 2-5: SSA and derivates.

Changes different from SSA are highlighted in red.

2.5 Overview of Pladienolide B

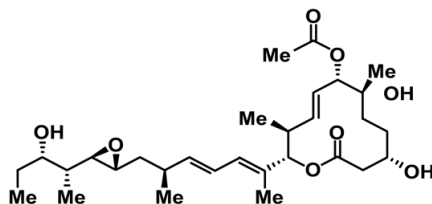
A group of Pladienolides were derived from *Streptomyces platensis* (Pladienolide A-G) (Sakai et al., 2004a; Sakai et al., 2004b). Pladienolide B (PB) demonstrated the strongest anti-tumor activity in *in vitro* and *in vivo* studies (Mizui et al., 2004; Kotake et al., 2007). PB is the second most potent of SF3B1 inhibitors needing 0.09 μ M to inhibit splicing by half (Effenberger et al., 2016b). Tumor activity in mice that were xenografted with gastric cancer from human cells disappeared after two weeks after treatment with PB and also demonstrated apoptosis (Sato et al., 2014). The first clinical trials of PB were using derivative E7107 in 40 patients with solid tumors to identify dose-limiting toxicities and explore any side effects (Eskens et al.,

2013). The study confirmed that there was a decrease in mRNA levels in target genes. A concurrent study found blurred vision was a side effect of E7107, but vision was restored upon discontinuation of the drug (Hong et al., 2013). H3B-8800 is another PB derivative that was shown to selectively kill SF3B1 mutant leukemia cells and induce antitumor activity in xenograft leukemia models is also undergoing clinical trials (Seiler et al., 2018; Rioux et al., 2020). To date, PB has been the only SF3B1 inhibitor that has undergone clinical trials. One of the challenges of PB (Figure 2-6), such as with SSA is having a complex ring structure that makes it difficult to synthesize.

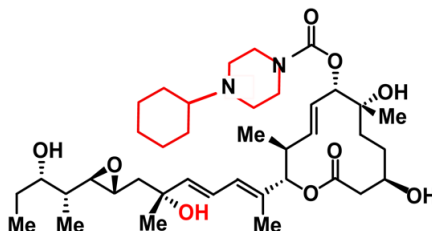
2.6 Overview of HB and derivatives

Herboxidiene (HB) was first discovered as a herbicide and was isolated from fermentation broth of *Streptomyces chromofuscus* (Miller-Wideman et al., 1992). HB was later discovered to have antitumor effects and is the least potent of all the drugs, needing 0.23 μ M to inhibit splicing by half (Sakai et al., 2002). In addition, synthesis of HB has been studied more than the biological implications, where medicinal chemists are pursuing derivatives that are feasible to create (Ghosh et al., 2014b) (Lagiseti et al., 2014). HB has been modeled inside SF3B to predict interactions with SF3B1 and PHF5A (Cretu et al., 2018). To date there are no herboxidiene analogs in clinical trials and more molecular studies of herboxidiene need to be done to better understand its mechanism of action. The Ghosh and Jurica labs recently discovered new HB analogs with anti-tumor properties as shown in Figures 2-7 and 2-8 (Ghosh et al., 2021).

PB



E7107



H3B-8800

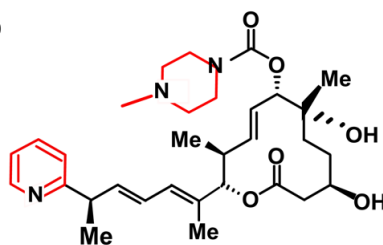
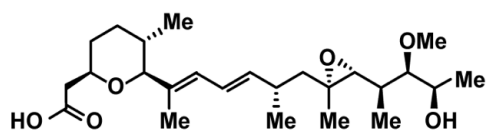


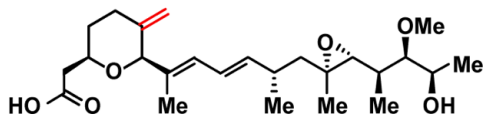
Figure 2-6: Pladienolide B and derivatives.

Changes different from PB are highlighted in red.

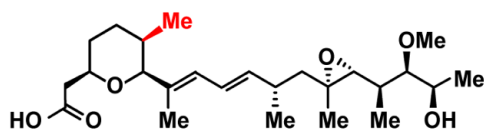
HB



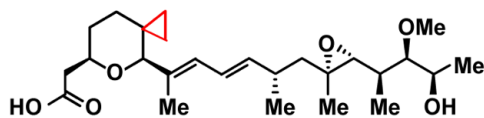
Compound 12



Compound 13



Compound 14



Compound 15

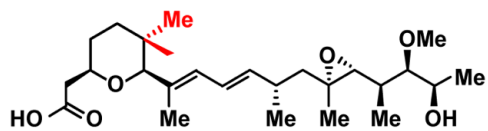


Figure 2-7: Herboxidiene and derivatives.

Changes different from HB are highlighted in red.

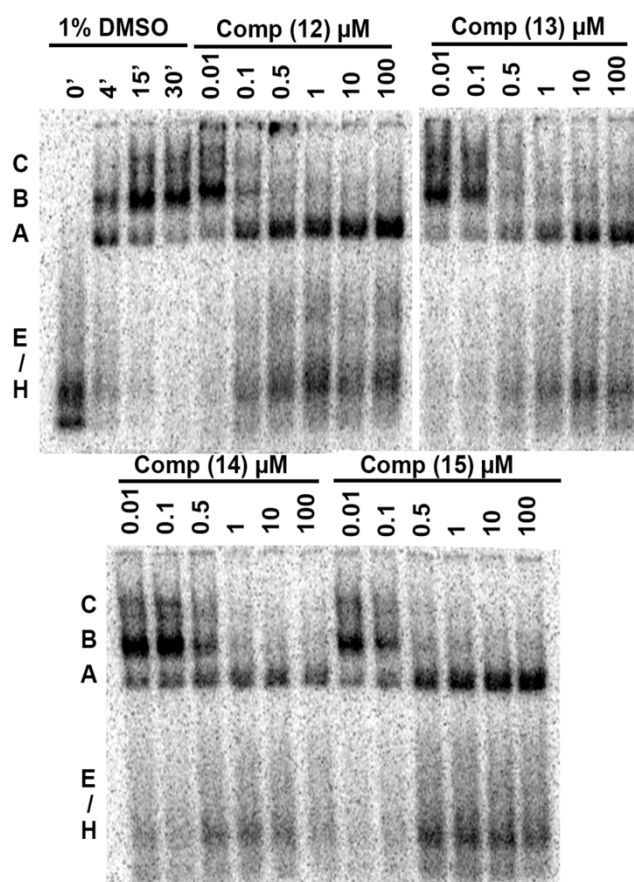


Figure 2-8: New Derivatives of herboxidiene inhibit spliceosome assembly.

Representative native gel analysis of spliceosome assembled for 0, 4, 15 and 30 min at 30°C in the presence of compounds 12,13,14 and 15 from Figure 2-7 with varying concentrations. The identities of the spliceosome complexes occur in the following order: H/E ->A->B->C. (Ghosh et. al. 2021)

2.7 Challenges when creating SF3B1 inhibitors and contribution to the dissertation

One of the many challenges of synthesizing SF3B1 inhibitors is adding chemical features to certain regions of the molecule because the chemistry is not possible (Arai et al., 2014). Creating drugs involves multiple steps that can be time

consuming, high cost and low production. Compounds selected by nature for activity often contain complex shapes and functional groups. Finding a synthetic pathway to produce the product is not always feasible and does not always produce a high yield. For example, synthetically producing PB takes a series of 24 steps (Ghosh and Anderson, 2012). Nature has developed bacterial enzymes to carry out these steps with precise stereochemistry. For example, Machida et al. studied the gene cluster organization synthesis of PB which has a simpler pathway than when done synthetically (Machida et al., 2008). Once a new drug product is screened a biological profile of the drug is needed which can be very costly (Blakemore et al., 2018). Creating enantiomers and bioproducts is also a concern as well as drug purity. Drug storage and creating a stable environment for longevity depends on the properties of the drug and what vehicle will be used for patient delivery. Lastly, we know some aspects of how the drugs work, but do not fully understand how they bind and how they interfere with SF3B. We know that SF3B inhibitors stop cell growth, mutations close to the SF3B binding pocket are resistant to inhibitors, but so far, all this evidence leads to splicing. Lastly, drugs that do not inhibit splicing are correlated to drugs that do not inhibit cell growth. Part of my dissertation will be focused on better understanding the chemical features of herboxidiene. I will specifically be focusing on the ring and will examine how chemical changes in C1 and C6 affect binding and inhibition to SF3B1.

Chapter 3: Herboxidiene features that mediate conformation-dependent SF3B1 interactions to inhibit splicing

3. 1Abstract

Small molecules that target the spliceosome SF3B complex are potent inhibitors of cancer cell growth. The compounds affect an early stage of spliceosome assembly when U2 snRNP first engages the branch point sequence of an intron. Employing an inactive herboxidiene analog (iHB) as a competitor, we investigated factors that influence inhibitor interactions with SF3B to interfere with pre-mRNA splicing *in vitro*. Order-of-addition experiments show that inhibitor interactions are long lasting and affected by both temperature and the presence of ATP. Our data are also consistent with the model that not all SF3B conformations observed in structural studies are conducive to productive inhibitor interactions. Notably, SF3B inhibitors do not impact an ATP-dependent rearrangement in U2 snRNP that exposes the branch binding sequence for base pairing. We also report extended structure– activity relationship analysis of the splicing inhibitor herboxidiene. We identified features of the tetrahydropyran ring that mediate its interactions with SF3B and its ability to interfere with splicing. In the context of recent structures of SF3B bound to inhibitor, our results lead us to extend the model for early spliceosome assembly and inhibitor mechanism. We postulate that interactions between a carboxylic acid substituent of herboxidiene and positively charged SF3B1 side chains in the inhibitor binding channel are needed to maintain inhibitor occupancy while counteracting the SF3B transition to a closed state that is required for stable U2 snRNP interactions with the intron.

Graphic Summary:

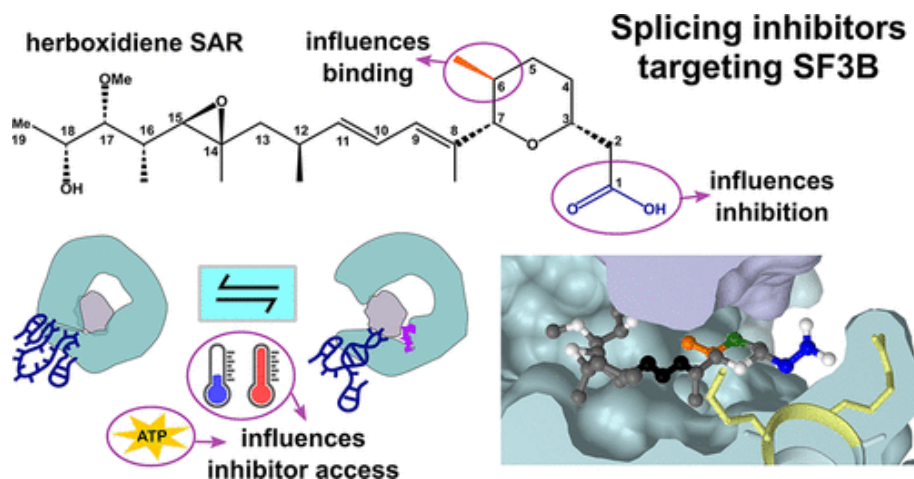


Figure 3-1: Temperature and ATP influences inhibitor access to SF3B

Keywords: SF3B, pre-mRNA splicing, SF3B inhibitors, herboxidiene analogs

3.2 Introduction

The spliceosome is responsible for removing introns from gene transcripts in eukaryotes to generate messenger RNAs (mRNA). It assembles on each intron to be removed from a transcript from five U-rich small nuclear RNAs complexed in ribonucleoproteins (snRNPs), which join with dozens of additional proteins through a complicated series of interactions and structural rearrangements. In early spliceosome assembly, U2 snRNP, which consists of U2 snRNA, core proteins and the SF3A and SF3B multi-protein complexes, joins the intron to form the A-complex spliceosome. U2 snRNA base pairs with the neighboring nucleotides of the branch point sequence (BPS) to specify an adenosine residue near the end of intron as the branch point (Plaschka et al., 2018; Parker et al., 1987). Because the 3' splice site is typically the first AG dinucleotide within a certain downstream distance from the branch point,

selection of the BPS also determines the end of introns (Chen et al., 2000; Taggart et al., 2012; Smith et al., 1989; Smith et al., 1993; Reed, 1989). Proteins involved in BPS selection, including SF3B components, are frequently mutated in some cancers and dysplasia, which suggests a role for intron definition in carcinogenesis (Hubert et al., 2013; Quesada et al., 2011; Yoshida et al., 2011; Papaemmanuil et al., 2011). Specific SF3B1 cancer mutations are linked to use of an aberrant branch point and 3' splice site in some transcripts, indicating that SF3B1 normally helps ensure fidelity of BPS selection (Tang et al., 2020; Darman et al., 2015; Alsafadi et al., 2016).

Recent cryo-EM structural models of the spliceosome captured at the earliest stage of assembly provide some clues for how SF3B1 participates in BPS recognition (Maji et al., 2019; Plaschka et al., 2017; Plaschka et al., 2018; Bai et al., 2018). The N- and C-terminal regions of the central C-shaped HEAT-repeat domain of SF3B1 come together and appear to clamp onto the branch helix formed by U2 snRNA and the intron. This conformation sequesters the bulged branch point adenosine into a pocket formed between PH5FA and SF3B1 HEAT repeats 15 and 16. Interestingly, in structures of U2 snRNP and isolated SF3B protein complex, the same domain exhibits a more open conformation that hinges at the same two HEAT repeats (Cretu et al., 2016; Zhang et al., 2020). Together, these structures imply that closing the SF3B clamp is a critical step in BPS selection.

Pladienolide B (PB), spliceostatin A (SSA) and herboxidiene (HB), first identified as potent inhibitors of tumor cell growth, are natural products that target SF3B and interfere with spliceosome assembly as U2 snRNP joins the intron to form

the spliceosome A-complex (Mizui et al., 2004; Kotake et al., 2007; Roybal and Jurica, 2010; Corriero et al., 2011; Folco et al., 2011; Effenberger et al., 2014). Structures of SF3B bound to PB revealed the inhibitor cradled in a channel between PHF5A and SF3B1 HEAT repeats 15 and 16 in the open conformation and the inhibitor is proposed to block SF3B closing (Finci et al., 2018; Cretu et al., 2018). In structures where SF3B1 is closed over the branch helix, several residues that contact the inhibitor are rearranged to form the pocket for the branch point adenosine, which effectively eliminates the inhibitor channel.

We previously reported that splicing inhibition by PB, SSA and herboxidiene can be masked by addition of an excess of some inactive analogs regardless of the structural family (Effenberger et al., 2016b). We hypothesized that the inactive analogs compete for the inhibitor channel but lack a chemical feature that is required for either more stable binding or interfering with SF3B function. We test the model in this study with a systematic series of analogs and conclude that SF3B1 interactions with the C1 carboxylic acid of herboxidiene are essential for the inhibitor to maintain binding in the context of SF3B closure over the branch helix. We also find that all SF3B inhibitors exchange very slowly relative, which enabled us to investigate factors that influence inhibitor interactions via competition studies. Our evidence points to SF3B conformation controlling access to the inhibitor binding channel, which is further regulated by an ATP-dependent event.

By differentiating chemical features of herboxidiene that contribute to binding and inhibitory activity, our results will support its therapeutic development. Already,

derivatives of PB and SSA show chemotherapeutic promise by decreasing the volume of human tumors implanted in mice and repressing expression and oncogenic splicing variant that confers chemotherapy resistance (Hong et al., 2013; Yoshikawa et al., 2020; Seiler et al., 2018). However, none have passed clinical trials (Eskens et al., 2013; Hong et al., 2013). Improvements based on structure activity relationship (SAR) studies are hampered by the structural complexity of these natural products. Our results here demonstrate that tuning the activity of herboxidiene, which has a somewhat simpler structure relative to SSA and PB, is more feasible and enables a deeper investigation into SF3B mechanism needed to realize the promise of splicing inhibitors for human health

3.3 Results and Discussion

Order of addition affects competition between SF3B inhibitors and inactive analogs

We previously showed that when 1 μ M herboxidiene, PB or SSA alone is included in an *in vitro* splicing reaction, splicing products are not detected. However, when 100 μ M of an inactive analog of herboxidiene (iHB) is added simultaneously, splicing products are produced at levels nearly equivalent to control reactions with no added inhibitor. We tested whether the order of addition affects competition between SF3B inhibitors and iHB competitor. We reasoned that if inhibitor interactions exchange rapidly with SF3B, then incubating the inhibitor in nuclear extract prior to adding excess inactive competitor would have no effect on the competitor's ability to rescue *in vitro* splicing from inhibition. Alternatively, if the inhibitor exchanges slowly or interferes irreversibly with SF3B function, then excess inactive competitor added

after the inhibitor would not be able to replace it and result in low splicing efficiency. To distinguish between these two possibilities, we incubated 1 μ M PB in nuclear extract for 10 minutes (binding phase), and then added 100 μ M iHB for an additional 10 minutes (competition phase) (Figure 2A). We then tested the nuclear extracts for *in vitro* splicing efficiency (splicing phase). In control experiments, nuclear extract treated with PB or SSA followed by DMSO yielded no splicing products (Figure 2B lanes 3 and 6, and 2C). An excess of inactive competitor iHB added before inhibitor PB or SSA rescues splicing efficiency to the level of DMSO controls, consistent with previous results with simultaneous addition (Figure 2B lanes 5 and 8, and 2C) (Effenberger et al., 2016B). In contrast, when PB or SSA is incubated with nuclear extracts before addition of excess iHB competitor, splicing efficiency is greatly reduced, although not completely lost relative to the inhibitor alone (Figure 2B, lanes 3-5 and 6-8, and 2B). We also tested less potent inactive competitor analogs of PB and SSA in the same manner with similar outcome (Supplemental Figure 2). Ordered competition with herboxidiene does yield a strong difference in splicing inhibition, which is consistent with its lower potency relative to SSA and PB (Supplemental Figure 2). Although our assay does not directly measure binding, these results are consistent with a very slow off-rate for PB and SSA, which opened the door to using the competition assay to assess factors that affect the interaction between SF3B and its inhibitors.

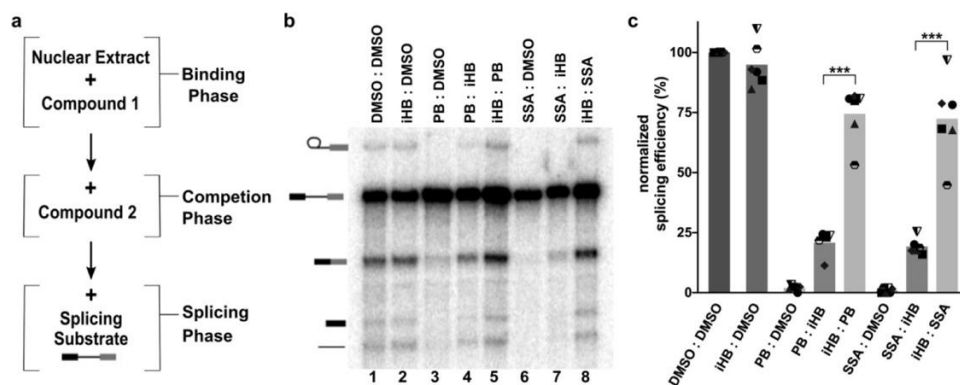


Figure 3-2. Order of addition affects competition between SF3B inhibitors and an inactive herboxidiene analog.

A) Schematic of order of addition assay. **B)** Representative denaturing gel analysis of *in vitro* splicing. Binding and competition phases were 10 min at 4 °C with DMSO, iHB (100 μM), PB (1 μM), or SSA (1 μM) and denoted Compound 1: Compound 2. The splicing phase was 30 min at 30 °C. Band identities are illustrated on the left as (top to bottom): lariat intron intermediate, pre-mRNA substrate, mRNA product, 5' exon intermediate and linear intron product. Chemical structures of compounds are illustrated in Supplemental Figure 1. **C)** Splicing efficiency quantified from denaturing gels plotted relative to DMSO control. Mean normalized splicing efficiency is displayed as bars, with experimental replicate values represented by different shape. *** $p < 0.001$.

Inhibitor interactions with SF3B are modulated by temperature

Because structural models imply that an open SF3B1 conformation is required for inhibitor binding (Plaschka et al., 2018; Cretu et al., 2018), we reasoned that temperature may modulate SF3B conformational dynamics and affect accessibility of the inhibitor channel. We repeated the same order of addition assay and compared the effect of incubating inhibitors during the binding and competition phases at 4°C vs. 30°C, while the splicing phases remained at 30°C (Figure 3A). In the absence of competition, incubation temperature has no significant effect on splicing or splicing

inhibition (Figure 3B, C). The result is different in the context of competition. When SSA, PB or herboxidiene is first incubated in nuclear extract at 30°C before addition of excess iHB competitor, the extract's splicing efficiency is lower compared to when they are first incubated at 4°C (Figure 3A lanes 6 vs 7, 8 vs 9 and 10 vs 11). The effect of a higher temperature incubation providing inhibitors a stronger competitive advantage relative to lower temperature incubation also holds for less potent inactive competitor analogs of PB and SSA (Supplemental Figure 3). The difference is consistent with differential accessibility of the inhibitor binding channel in SF3B depending on its conformation. We speculate that higher temperature favors the SF3B1 open conformation to give the inhibitor more opportunity to interact with SF3B before the competitor is added, which enables the inhibitor to prevent splicing when substrate is introduced into the extract.

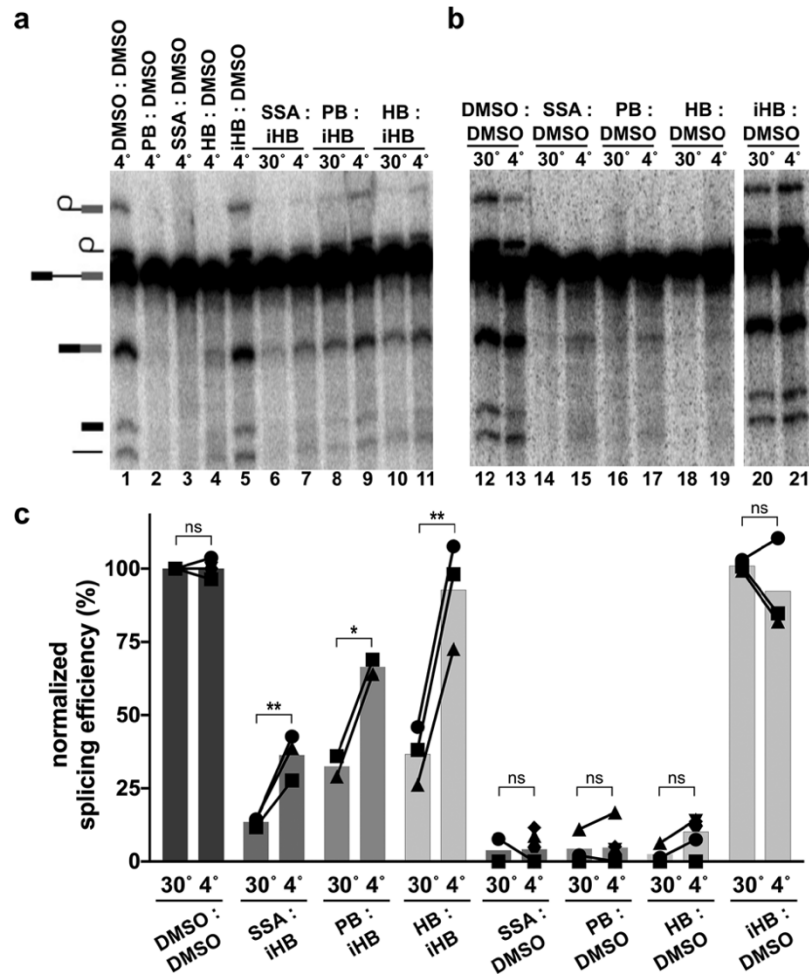


Figure 3-3. Temperature affects competition between SF3B inhibitors and inactive analogs.

(A and B) Representative denaturing gels as described in Figure 1. Binding and competitions phases were 10 min at 4 or 30 °C with DMSO, HB (1 μM), PB (1 μM), SSA (1 μM), or iHB (100 μM). C) DMSO, HB (1 μM), PB (1 μM), SSA (1 μM), or iHB (100 μM). (c) Splicing efficiency quantified from denaturing gels as described in Figure 1. n.s. = $p \geq 0.033$, * $p < 0.033$, ** $p < 0.002$.

Temperature-dependent interactions with SF3B are not modulated by ATP

The mechanisms controlling SF3B conformation are not fully understood. A recent cryo-EM structure of the U2 snRNP revealed SF3B in the open conformation with the inhibitor binding channel accessible (Zhang et al., 2020). Notably, the RNA-dependent ATPase DDX46 (human ortholog of yeast Prp5) contacts SF3B1. In the competition assays described above, we included ATP during inhibitor incubation in the nuclear extracts. To test the hypothesis that the temperature dependent effects on inhibitor interactions with SF3B were mediated by an ATP-dependent event, we repeated the splicing assay but excluded ATP during the competition phase of the experiment. Surprisingly the absence of ATP during the competition phase did not abolish the effect of temperature on splicing inhibition. ATP-depleted extracts incubated with inhibitor at 30°C followed by excess competitor still exhibited lower splicing efficiency relative to competition at 4°C (Figure 4A lanes 4 vs. 5, 6 vs. 7, and 4B). We conclude that SF3B1's ability to transition from a closed conformation that is refractory to inhibitor binding, to an open conformation that is available for inhibitor binding is influenced by temperature. Nevertheless, the presence of ATP does favor inhibitor interactions 30°C (Figure 4A lanes 4 vs. 6, and 3B), meaning that ATP promotes inhibitor access to SF3B independent of temperature, possibly through the activity of DDX46.

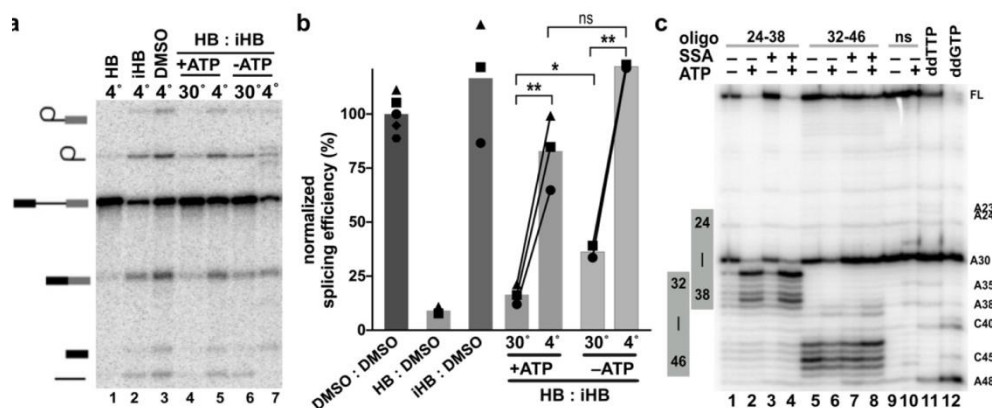


Figure 3-4. Temperature-dependent modulation of SF3B inhibition is independent of ATP.

A) Representative denaturing gel as described in Figure Binding and competitions phases were 10 min with 1 μ M HB or 100 μ M iHB. **B)** Splicing efficiency quantified from denaturing gels as described in Figure 1. **C)** Primer extension analysis of targeted DNA-oligo mediated RNase H digestion of U2 snRNA in nuclear extracts. Extracts were incubated \pm ATP and 1 μ M SSA for 10 min at 30 $^{\circ}$ C prior to addition of oligos complementary to the indicated nucleotides. ns = nonspecific oligo, ddTTP and ddGTP = sequencing lanes.

ATP-dependent changes in U2 snRNA BBS accessibility are not influenced by SF3B1 inhibitors

Stable incorporation of U2 snRNP in A-complex to establish the branch helix requires at least one ATP-dependent step (Zhuang and Weiner, 1989; Wu and Manley, 1989; Konarska and Sharp, 1987). ATP is also required for U2 snRNP association with pre-mRNA in the presence of both SSA and PB to form an unstable A-like complex in which the branch helix is not fully formed (Roybal and Jurica, 2010; Corrienero et al., 2011; Effenberger et al., 2016a). U2 snRNP conformation is also regulated by ATP (Abu Dayyeh et al., 2002; Black et al., 1985; Folco et al., 2011). Folco *et al*

reported that the PB analog E7107 inhibits U2 snRNPs ability to engage an oligo containing the branch sequence, but that inhibition is bypassed by an ATP-dependent rearrangement of the snRNP (Folco et al., 2011). We hypothesized that the small improvement of inhibitor competition conferred by the presence of ATP at 30°C is due to the same ATP-dependent rearrangement. To test this idea, we examined U2 snRNA accessibility in the presence and absence of ATP and SF3B inhibitor.

Upon addition of DNA oligos that are complementary to regions accessible for base pairing, endogenous RNase H in nuclear extract cleaves RNA in any RNA/DNA hybrids that form. We tested DNA oligos targeting U2 snRNA nucleotides between Stem I and Stem IIa, and mapped cleavage sites using primer extension. As predicted by previous studies, cleavage efficiency changes in some regions when extracts are first incubated with ATP (Black et al., 1985). The most predominate change is an increase in cleavage at nucleotides 33 through 38 with an oligo complementary to nucleotides 24-38 (Figure 4C lanes 1-4). Notably, these nucleotides are the GUAGUA nucleotides of the branch binding sequence that forms base pairs with an intron. They also sit in the loop region of the branchpoint-interacting stem loop (BSL) as recently visualized in the U2 snRNP structure (Zhang et al., 2020). Because ATP increases RNA cleavage in this region, an unwinding of the BSL, potentially by DDX46, is a possible explanation for the increased accessibility. Alternatively, release of DDX46 from the snRNP may allow access to the DNA oligo probe. Surprisingly, the SF3B inhibitor SSA does not interfere with the ATP-dependent changes in cleavage (Figure 4C). It is therefore possible that exposing the branch binding sequence of U2 snRNA mediates

the ATP-requirement for U2 snRNP associates with an intron in the presence of inhibitor. The result also suggests that this event is independent of a transition from open to closed SF3B conformation, although we cannot rule out that an open SF3B is required. Notably, the previously described ATP-dependent conformational change in U2 snRNP affected by SF3B inhibitors remains to be characterized (Folco et al., 2011).

Inactive analogs of SF3B inhibitors only lose some their competitive advantage over time

The idea that splicing inhibitors preventing SF3B closure raises an interesting question: How does iHB block SF3B inhibitor action, presumably by competing for the SF3B channel, while at the same time not affect splicing? One possible explanation is that the inactive compound exchanges rapidly from the binding site in comparison with the apparent slow off-rate for active compounds suggested by our order of addition experiments. If true, when inactive compound is incubated in extract before adding inhibitor, then competition will not show the same temperature dependence, because the inactive compound be quickly replaced by an active inhibitor with the final shift to 30°C for the splicing reaction. Furthermore, the ratio of active to inactive compound should affect both the extent and rate of competition. To test these predictions, we repeated the order of addition experiment at both 4° and 30°C, but added 100µM, 10µM or 1µM iHB first for 10 minutes, and followed with 1 µM SSA for another 10 minutes. As predicted, splicing is rescued to the same level at both temperatures when an excess of inactive competitor is added first (Figure 5A lanes 3 vs. 4, 6 vs.7,9 vs. 10 and 5B), and holds for competitions with inactive analogs of PB and SSA followed by herboxidiene, PB or SSA (Supplemental Figure 4a, b, c). When at a 1:1 ratio splicing

was largely inhibited, but the small amount of splicing rescue was slightly higher for competition at 4°C relative to 30°C. This result is consistent with SSA having increased access to SF3B at the higher temperature as the inactive competitor leaves.

Differences in exchange rates for inactive competitors vs. SF3B inhibitors also predict that extending competition for a longer period of time should result in decreased splicing rescue when inactive competitor is followed by an inhibitor that has much slower exchange rate. We tested this expectation by incubating iHB in nuclear extract for 10 minutes at 30°C and then adding PB to compete for 10, 30 or 90 minutes (Figure 5C lanes 1-4, 5-8, 9-12 respectively and 5D). To further bias competition toward the active inhibitor, we used a ratio of 10:1 iHB to PB. Although splicing efficiency decreases somewhat with longer competition, iHB's competitive advantage still remains after 90 minutes with only a 50% reduction relative to shorter competitions of 10 or 30 minutes (Figure 5C, D). Coupled with its ability to also rescue splicing at relatively low concentrations (1:1 and 1:10), it appears that even though iHB's exchange rate from SF3B is higher than active inhibitors, it not rapid enough to explain why iHB has no effect on splicing.

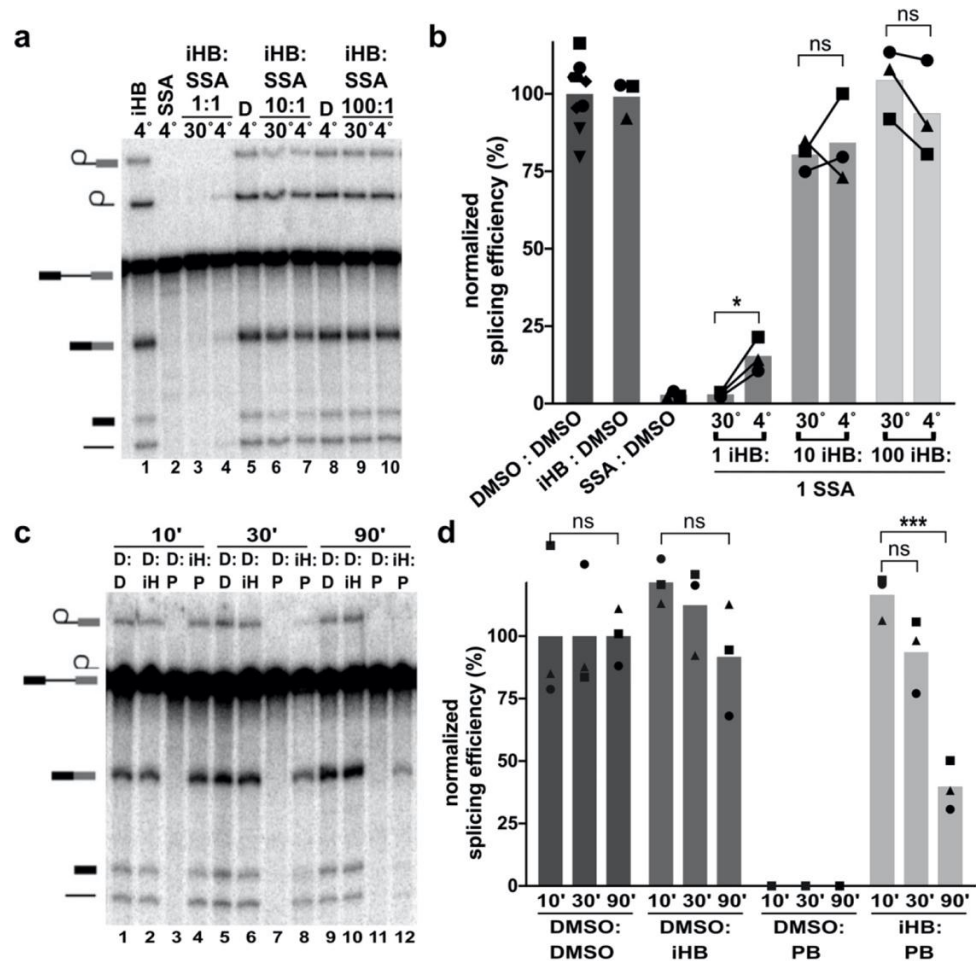


Figure 3-5. SF3B inhibitors exchange more slowly than inactive analogs.

A) Representative denaturing gel as described in Figure 1. Binding and competitions phases were 10 min with 1, 10, or 100 μ M iHB and 1 μ M SSA. **B)** Splicing efficiency quantified from denaturing gels as described in Figure 1. **C)** Representative denaturing gel with 10 min binding phase and varying length competitions phases at 30 $^{\circ}$ C. D = DMSO, iH = iHB, P = PB. **D)** Splicing efficiency quantified for **(C)**.

Chemical features of herboxidiene differentially impact splicing inhibition and competition

To further explore the chemical features of herboxidiene (**1**) important for splicing inhibition and competition we tested a series of analogs in which we varied the substituents at C1 and C6 positions (see Figure 6 for compound modifications numbered **(1)**-**(20)**). The inactive herboxidiene analog iHB (**14**) that we used for our competition assays differs from the active parent compound herboxidiene at two positions: an additional hydroxyl group at C5 of the tetrahydropyran ring, and conversion of the C1 carboxylic acid to its methyl ester. The C1 methyl ester is likely responsible for the lack of splicing inhibition, because the presence of the C5 hydroxyl group alone (**2**) has a minimal effect on compound activity (Ghosh et al., 2014b). The parent compound, herboxidiene (**1**), has an IC₅₀ value for *in vitro* splicing of 0.3 μM (Ghosh et al., 2014b). Removing the methyl group at C6 (**3**) or replacement with a methylene group (**4**) had essentially no effect on compound activity, as their IC₅₀ values remain sub-micromolar and comparable to herboxidiene (**1**). Flipping the chirality of the methyl group (**7**), creating a di-methyl (**6**) or cyclopropane at C6 (**8**) each resulted in >4-fold decreased inhibitory activity, while addition of a methyl ether (**9**) dropped activity >10-fold. Inclusion of an epoxy group (**17** and **18**) or a dichlorocyclopropane functionality (**15**) resulted over 500-fold decreased activity with an IC₅₀ value greater than 100 μM, which we classify as inactive. From these results, we conclude that the presence and orientation of the methyl group at C6 in herboxidiene is not crucial for the inhibitor's activity. However, increasing the size of the group at that position does

have a deleterious effect. We also tested some of alterations at C6 (dimethyl, cyclopropane, methylether, dichlorocyclopropane) in combination with a methyl ester at C1. In this context, all compounds showed no activity at 100 μ M, further supporting a critical role for the carboxylic acid functionality at C1. Notably, substitution of the carboxylic acid at C1 with carboxamide (**10**) along with an additional hydroxyl at C5 (**12**) strongly reduced splicing inhibition (>10-100-fold) but did not completely inactivate the compound in our assay system. Converting the C1 carboxylic acid to its hydroxymethyl derivative (**11**), in the context of the normally benign C5 hydroxyl addition, also strongly affected activity. We next asked at what level inactive herboxidiene analogs are able to compete with an inhibitor. Addition of most inactive analogs at 100 μ M rescued >95% of splicing activity normally completely inhibited by 1 μ M PB, although rescue was slightly reduced with two compounds that had both a methyl ester group at C1 and bulky adduct at C6. At a 10:1 ratio, compounds with larger adducts at C6 (compounds **15-20**) again yielded lower splicing rescue.

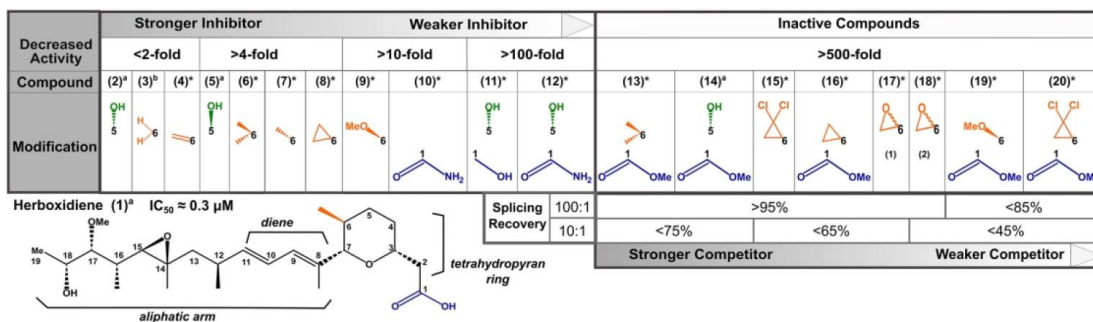


Figure 3-6. Structure–activity relationships for herboxidiene activity and SF3B interaction.

Summary of SAR results relative to the chemical structure of herboxidiene with modifications colored by their location and grouped by the magnitude of effect on inhibitor activity relative to the parent compound. Compounds with >500-fold decrease in inhibitory activity were tested for their ability to rescue splicing activity with 1 μM active splicing inhibitor at 100-fold and 10-fold excess. * indicates compounds new to this study. a Refer to ref 39. b Refer to ref 40.

Modeling herboxidiene interactions with SF3B

We modeled herboxidiene into the PB binding site of the SF3B crystal structure by overlaying the aliphatic arm and diene, and placing the carboxyl group over the ester of PB's macrolide ring similar to Cretu *et al.* (Cretu *et al.*, 2018). The model predicts that groups at C1 and C6 positions interact with residues from the U2 snRNP proteins PHF5A and SF3B1 (Figure 7A). The methyl group at C6 is close to a surface of PHF5A that remains relatively static in the context of SF3B1 closing. Compounds with larger adducts at this position (for example, **15**) would sterically clash, which explains both their decreased potency as splicing inhibitors and decreased ability to compete with active inhibitors. The carboxyl group at C1 interacts with residues in HEAT repeat 15 of SF3B1, which undergo a large structural shift when SF3B1 closes to engage the branchpoint adenosine of an intron. Modifications at C1 decrease herboxidiene's

activity, showing that the position is important for inhibition, but have less impact on competition. Extended competitions in which inactive competitor is added first are consistent with iHB (**14**) having a higher exchange rate from the inhibitor binding channel relative to strong inhibitors. Still, why the inactive compounds are able to block SF3B inhibitors for extended periods of time, but do not block engagement of the intron at the same level is puzzling. It may be that our changes at C1, which removes potential hydrogen bonding partners, do not strongly affect affinity for the inhibitor binding channel present in an open SF3B1. Instead, a carboxylic acid at C1 may be important for stabilizing the position of nearby positively charged side chains and prevent their normal rearrangement to contact the intron during SF3B1 closing. Consistent with this idea, SF3B1 mutants have been identified as resistant to PB and herboxidiene (Yokoi et al., 2011; Butt et al., 2019), and these mutations map to the positively charged amino acids (K1070, K1071, R1074, R1075) that are situated adjacent to C1 in our model (Figure 7B, C). We speculate that without the carboxylic acid functionality to compete with the SF3B1 conformational change required for intron engagement, inactive competitors are effectively ejected from SF3B upon closing. We aim to test this model in the future with inactive herboxidiene analogs that are engineered with a cross-linking group to stabilize their occupancy in the channel.

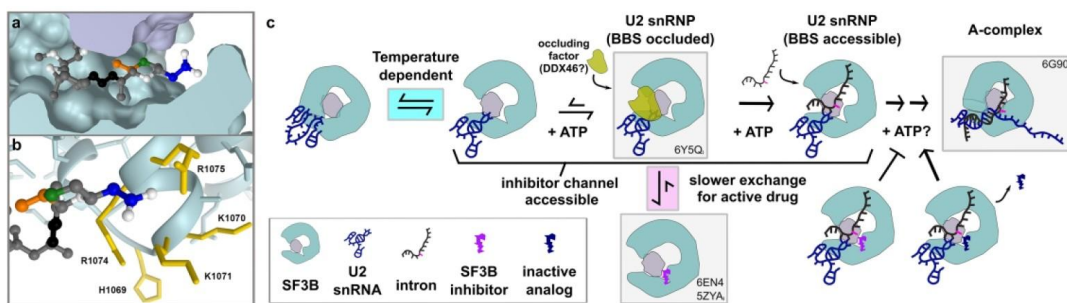


Figure 3-7. Model of early spliceosome assembly and SF3B inhibition.

A) Model of herboxidiene bound to SF3B inhibitor channel between SF3B (teal) and PHF5A (purple). Positions are colored as follows: C1, blue; C5, green; C6, orange; diene, black. **B)** Side chains located near the modeled position of herboxidiene C1. Mutations of labeled residues in yellow confer resistance to Pladienolide B or herboxidiene. **C)** Model of early spliceosome assembly steps and SF3B inhibitor action.

3.4 Conclusion

The ability of iHB (**14**) to compete with inhibitors provides a unique way to study the parameters that affect inhibitor activity, and by extension their molecular target. Through order of addition experiments, we found that inhibitor interactions with SF3B are long lived and that access to the inhibitor channel changes in response to temperature and an ATP-dependent event. We also found that SF3B inhibitors do not interfere with an ATP-dependent rearrangement that exposes U2 snRNA. These results combined with previous studies lead us to expand the model of U2 snRNP addition to the spliceosome (Figure 7C). Although SF3B inhibitors do not prevent U2 snRNP from joining an intron in an A-like splicing complex (Roybal and Jurica, 2010; Corrienero et al., 2011; Folco et al., 2011), the complex is less stable relative to the real A-complex, and likely has not yet completely formed the branch helix (Corrienero et al., 2011; Effenberger et al., 2016b). Notably even in the presence of inhibitor, ATP is required

for U2 snRNP's interaction with an intron. We hypothesize that this event may be related to the rearrangement that leads to increased accessibility of the U2 snRNA branch binding sequence. A recent cryo-EM structure revealed a population of U2 snRNPs in which the protein HTATSF1 is situated between the open "jaws" of SF3B1, while the branch binding sequence of U2 snRNA is folded in the BSL and surrounded by both HTATSF and DDX46 (Zhang et al., 2020). It may be that DDX46 uses ATP to promote these interactions to help stabilize the SF3B1 open conformation necessary for inhibitor occupancy of the binding channel. We hypothesize that an ATP-dependent restructuring of U2 snRNP, potentially involving the removal of HTATSF1 and/or release of DDX46 would allow an intron initial access to U2 snRNA to form the A-like complex stalled by SF3B inhibitors. We also suspect additional ATP-dependent rearrangements in U2 snRNP are required for branch helix formation given the extensive rearrangements of RNA/RNA and RNA protein interactions that must take place for U2 snRNP to take on the structure observed in the cryo-EM model of A-complex (Plaschka et al., 2018). Nearly irreversible inhibitor interaction with SF3B prevents the transition to a closed SF3B1 conformation that is required to form or stabilize the branch helix. Nailing down the players and order of these interactions is the next challenge for splicing researchers, and SF3B inhibitors will likely continue to be important tools for helping to probe the process.

3.5 Materials and Methods

Synthesis of SF3B1 inhibitors and analogs

Synthesis of SF3B1 inhibitors and herboxidiene analogs (**2**), (**3**), (**5**) and (**14**), are published (Ghosh and Li, 2011; Ghosh and Anderson, 2012; Ghosh and Chen, 2013; Ghosh et al., 2014b; Ghosh et al., 2016). Herboxidiene analogs (**4**), (**6-3**) and (**15-20**) were synthesized and purities were assessed by HPLC (>90% pure). The details of synthesis are described in a separate publication (Ghosh et al., 2021).

***In vitro* splicing analysis**

Pre-mRNA substrate was derived from the adenovirus major late (AdML) transcript (sequence shown in Supplemental Figure 5). ³²P-UTP body-labeled G(5')ppp(5')G-capped substrate was generated by T7 run-off transcription followed by gel purification. Nuclear extract was prepared as previously described (Dignam et al., 1983) from HeLa cells grown in DMEM/F-12 1:1 and 5% (v/v) newborn calf serum. Order of addition experiments started with 60 mM potassium glutamate, 2 mM magnesium acetate, 2 mM ATP, 5 mM creatine phosphate, 0.05 mg/ml tRNA, 50% (v/v) HeLa nuclear extract and first compound and incubated at 4°C or 30 °C. Next the second compound was added, and the mixture was incubated for 10, 30 or 90 minutes at 4°C or 30°C. Then, radiolabeled pre-mRNA was added to a final concentration of 10 nM and the mixture incubated at 30°C for 30 or 60 minutes. The RNA was isolated from the reactions and separated on a 15% (v/v) denaturing polyacrylamide gel. ³²P-labeled RNA species were visualized by phosphorimaging and quantified with ImageQuant software (Molecular Dynamics). Splicing efficiency was quantified as the

amount of mRNA relative to total RNA and normalized to a dimethyl sulfoxide (DMSO) control reaction. Results were analyzed using unpaired t-test (two-tailed) using GraphPad Prism version 9.0.1 for Mac, GraphPad Software, San Diego, California USA.

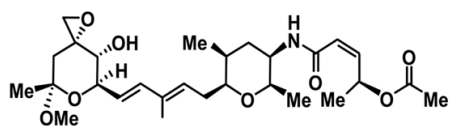
For experiments testing ATP-dependency, HeLa nuclear extract was first depleted of ATP by incubation at 30°C for 15 minutes. Following inhibitor competitions with and without added ATP (2 mM), additional ATP (2 mM) was included with pre-mRNA substrate to allow for splicing.

RNase H cleavage analysis

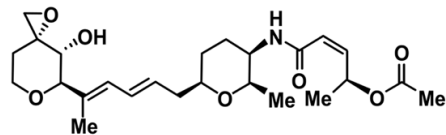
A mixture of 40% HeLa nuclear extract (depleted of ATP by incubating for 10 minutes at 30°C) 60 mM potassium glutamate, 2 mM magnesium acetate, 0.1 mg/mL tRNA with and without 2 mM ATP and 1 μ M SSA or DMSO was incubated for 10 minutes at 30°C. DNA oligos complementary to U2 snRNA 24-38 nt or 32-46 nt were added at 5 μ M and incubated for another 15 minutes at 30°C to allow for cleavage by endogenous RNase H. The oligos were degraded with addition of 1 μ L RQ1 DNase for 10 minutes at 30°C. RNA was isolated and used as template for reverse-transcription primer extension reactions by first annealing with a ³²P-radiolabeled primer complementary to U2 snRNA 97-117 nt. Reverse transcription reactions contained 50 mM Tris pH 7.9, 75 mM potassium chloride, 7 mM DTT, 3 mM magnesium chloride, 1 mM dNTPs, and 0.5 μ g reverse transcriptase (MMLV variant). After a 30-minute incubation at 53°C, DNA was isolated and separated on a 10% (v/v) denaturing polyacrylamide gel that was dried and visualized as described previously.

3.6 SUPPLEMENTAL DATA

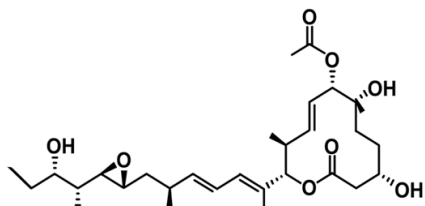
SSA



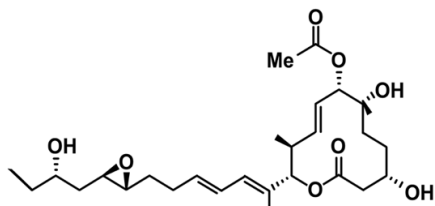
iSSA



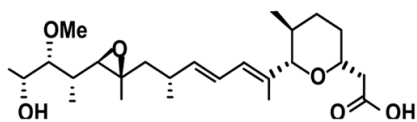
PB



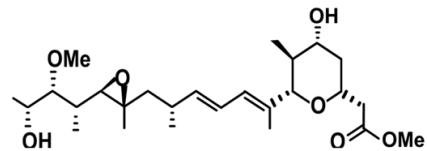
iPB



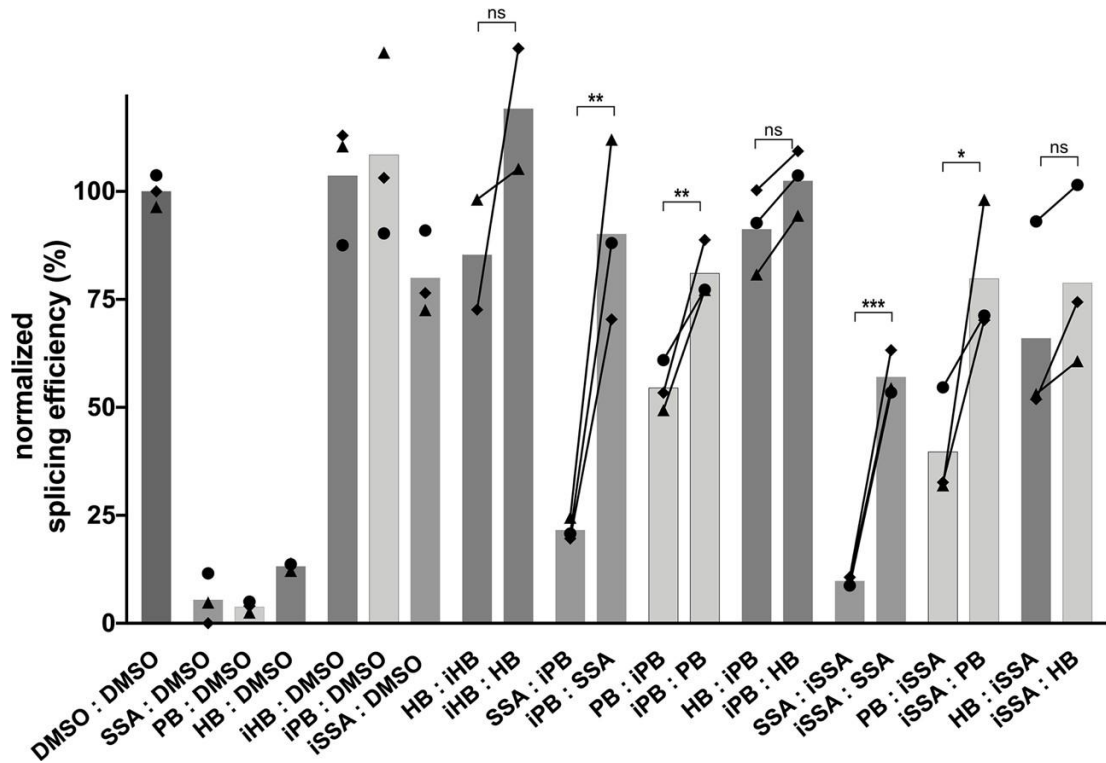
HB



iHB

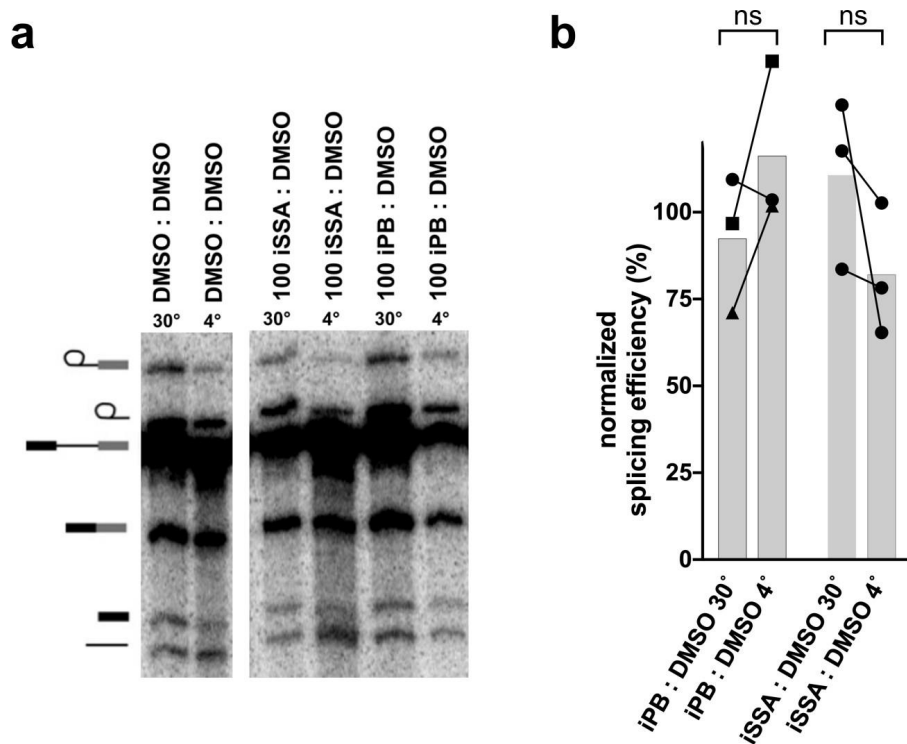


Supplemental Figure 3-1: Chemical structures of SF3B inhibitor analogs used in this study



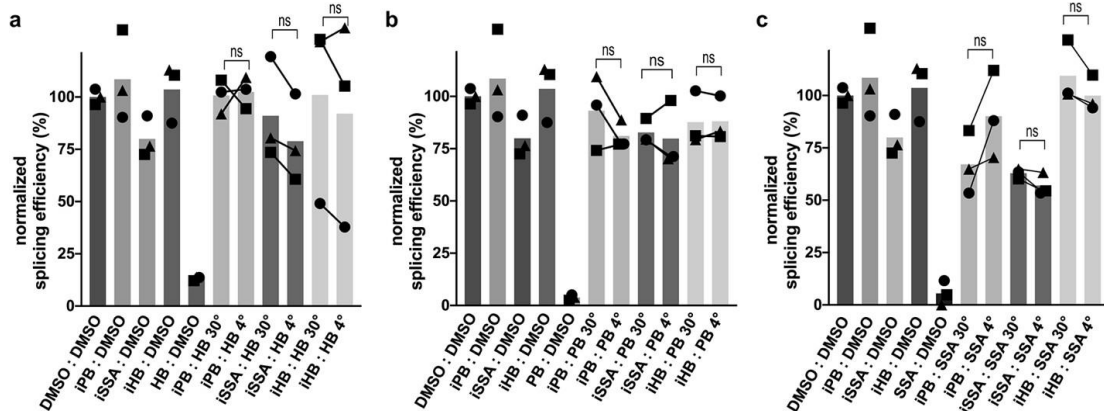
Supplemental Figure 3-2: Order of addition affects competition between SF3B inhibitors and inactive PB and SSA analogs

Quantification of *in vitro* splicing assays. Prior to addition of splicing substrate, nuclear extract was incubated at 4°C for 10 minutes with one of the compounds DMSO, herboxidiene (HB, 1µM), SSA (1µM) PB (1µM) iHB (100µM), iSSA (100 µM) or iPB (100 µM) followed by the indicated compound at same concentrations for another 10 minutes. Mean normalized splicing efficiency is displayed as bars, with experimental replicates values represented by different shape and linked to illustrate the difference in splicing rescue. *** p<0.001, ** p<0.002, * p<0.033, n.s. = p≥0.033



Supplemental Figure 3-3: Temperature affects competition with iSSA and iPB but not inactive and active compound controls

A) Representative denaturing gel analysis of *in vitro* splicing using nuclear extracts incubated at 4°C or 30°C for 10 minutes with DMSO or 100 μM (iSSA, iPB), followed by DMSO for 10 minutes. Band identities are illustrated on the left as (from top to bottom) lariat intermediate, lariat intron product, pre-mRNA substrate, mRNA product, 5' exon intermediate and linear intron product. **B)** Quantification of *in vitro* splicing assays. Mean normalized splicing efficiency is displayed as bars, with experimental replicates values represented by different shape and linked to illustrate the difference in splicing rescue.



Supplemental Figure 3-4: Temperature dependent inhibition of splicing depends on order of addition of excess inactive competitor

Quantification of *in vitro* splicing assays. Prior to addition of splicing substrate, nuclear extract was incubated at 4°C or 30°C for 10 minutes with one of the compounds DMSO, herboxidiene (HB, 1µM), SSA (1µM) PB (1µM) iHB (100µM), iSSA (100 µM) or iPB (100 µM) followed by addition of DMSO, herboxidiene HB (1 µM; panel A), SSA (1 µM; panel B) or iPB (100 µM; panel C) at the same concentration and temperature for another 10 minutes. Mean normalized splicing efficiency is displayed as bars, with experimental replicates values represented by different shape and linked to illustrate the difference in splicing rescue.

GAGACCGGCAGATCAGCTTGGCCGCGTCCATCTGGTCATCTAGGATCT
 GATATCATCGATGAATTCGAGCTCGGTACCCCGTTCGTCCTCACTCTCT
 TCCGCATCGCTGTCTGCGAGGGCCAGCGTAAAAGGTGAGTACTCCCTCT
 CAAAAGCGGGCATGACTTCTGCCCTCGAGTTATTAACCCTCACTAAAG
 GCAGTAGTCAAGGGTTTCCTTGAAGCTTTCGTGCTGACCCTGTCCCTTT
 TTTTCCACAGCTGCAGGTCGACGTTGAGGACAAACTCTTCGCGGTCTT
 TCCAGTACTCTTG

Supplemental Figure 3-5: Pre-mRNA sequence of substrate used in splicing for this study

Chapter 4: The effects of SF3B1 inhibitor on the U2 snRNP

4.1 Introduction

Motivation in studying the effects of SF3B1 inhibitor on the U2 snRNP

After splicing, the 12S form of the U2 snRNP is released from the lariat intron complex and must be remodeled and prepared for another round of splicing cycle in the 17S form. Biochemical studies suggest the 17S form is created when SF3B joins the 12S U2 snRNP generating the 15S U2 snRNP. Afterwards SF3A joins the 15S U2 snRNP to forming the 17 U2 snRNP (Brosi et al., 1993; MacMillan et al., 1994; Query et al., 1996; Will et al., 2001). Current structures give further evidence that assembly of the 17S U2 snRNP is regulated in a step-by-step manner (Lin and Xu, 2012; van der Feltz and Hoskins, 2019). Differential sedimentation of U2 snRNP in nuclear extract under 150mM KCl conditions determined that 12S U2 snRNP and 17S U2 snRNP could be separated (Behrens et al., 1993). However, only U snRNAs were visualized and not proteins. Will et al. repeated the experiment in which they took nuclear extract and looked at protein migration of SF3B and Prp5 (Will et al., 2002). We wanted to know if SF3B1 inhibitor could affect SF3B1 association with U2 snRNP. Our reasoning for doing this project was to further understand why splicing stalls at Complex A.

4.2 Results and discussion

SF3B1 inhibitor promotes 17S U2 snRNP in RNA Denaturing gels

As previously reported, 17S U2 snRNP and 12S U2 snRNP can be separated using differential sedimentation. We wanted to test if PB would affect association of

SF3B1 with U2 snRNP. The possible outcomes were 1) SF3B1 inhibitor promotes association of SF3B1 with U2 snRNP 2) SF3B1 inhibitor interferes with association of SF3B1 with U2 snRNP and 3) SF3B1 inhibitor has no effect on SF3B1 association with U2 snRNP. If the inhibitor promotes association then we would observe more 17S U2 snRNP. If the SF3B1 inhibitor interferes with association then we would observe 12S U2 snRNP. To test these predictions, we examined RNA of whole nuclear extract with and without PB using glycerol gradient fractionation. We examined the sedimentation shift of RNA using odd fraction samples in denaturing gels. In Figure 4-1A, DMSO control experiment demonstrates 12S U2 snRNP to be in fraction 5 and 17S U2 snRNP to be in fraction 11. However, there is a sedimentation shift when PB was added to nuclear extract. In Figure 4-1B, there is less U2 snRNA in fraction 5 and U2 snRNA intensity increased in fraction 11. In Figure 1C, demonstrate quantification analysis of denaturing gels 4 A and B. Other RNAs do not shift, for example 7SK, and U1 snRNA. An RNA loading control of known size was used. We conclude that SF3B1 inhibitor promotes association of SF3B and SF3A proteins with the 12S U2 snRNP to form 17S U2 snRNP.

SF3B1 inhibitor does not affect dissociation of U2 snRNP proteins.

Based on our previous result that SF3B1 inhibitor promotes SF3B1 association with U2 snRNP. We wanted to examine if a protein sedimentation shift would occur in the presence of PB. We chose two proteins each associated with U2 snRNP at different stages of assembly. SF3B3 is found in 15S and 17S U2 snRNP and SNRPB2 is a core U2 snRNP protein found in 12S, 15S and 17S U2 snRNP. We

hypothesized that in the presence PB, SNRPB2 and SF3B3 would co-sediment with 17S U2 snRNP. This time we took the even fractions and ran western blots. To our

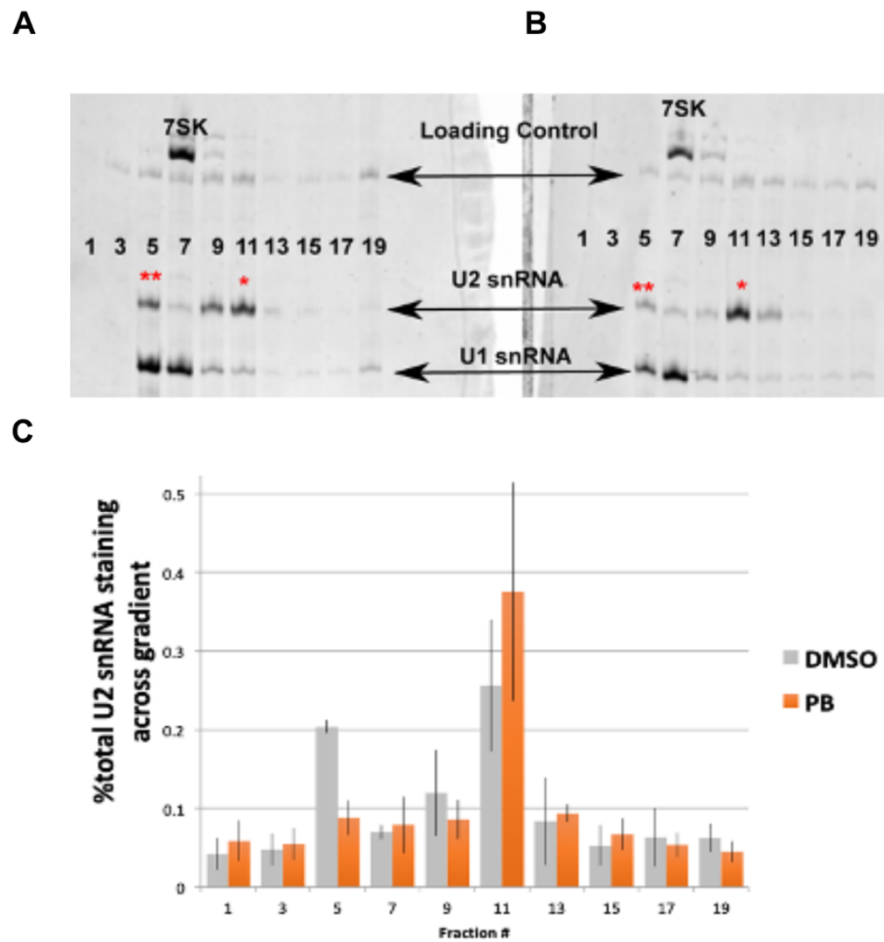


Figure 4-1: PB promotes formation of 17 U2 snRNP.

Representative denaturing gel of nuclear extract splicing conditions stained for all RNA with Sybr gold. Nuclear extract was incubated in 30°C along with different conditions prior to adding to glycerol gradients. Band identities are shown in the center top to bottom: 7SK, loading control, U2 snRNA, U1 snRNA and tRNA. **A)** Contains DMSO control **B)** 1μM of PB **C)** Quantification analysis of denaturing gels A and B. ** represents 12 U2 snRNP and * represents 17 U2 snRNP

surprise, the SF3B1 inhibitor had no effect on protein sedimentation profile. In figure 4-2 and 4-3, we still noted a separation between 12S and 17S U2 snRNP, but there were no differences in SF3B3 and SNRPB2 migration in the presence or absence of PB. This result conflicts with what we saw in RNA migration, differences in stability of 12S vs 17S U2 snRNP, but in proteins there is no effect with drugs.

SF3B3 (Full U2 snRNP) Protein

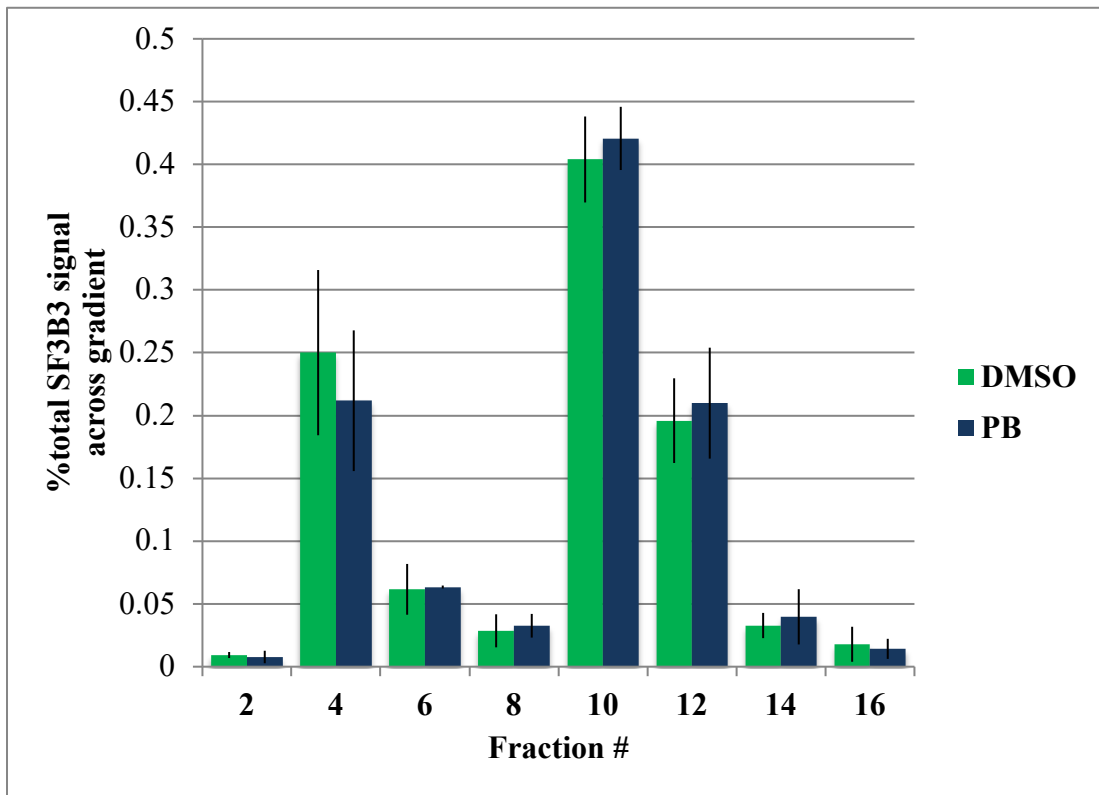


Figure 4-2: PB has no effect on SF3B3 migration.

Western blot analysis of even glycerol gradient fractions probed for SF3B3. Green represents DMSO control and blue fractions containing PB. Each fraction represents the % total signal across gradient.

SNRPB2 (U2 core) Protein

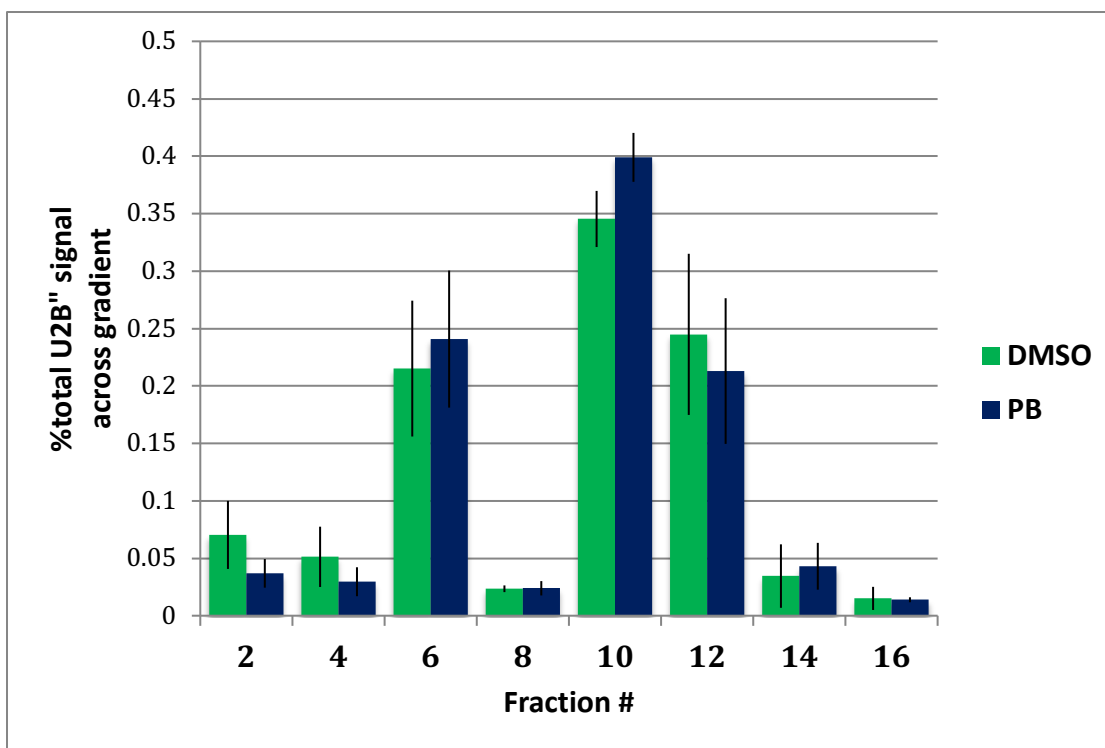


Figure 4-3: PB has no effect on SNRPB2 migration.

Western blot analysis of even glycerol gradient fractions probed for SNRPB2. Green represents DMSO control and blue fractions containing PB. Each fraction represents the % total signal across gradient.

Northern and Western blot of glycerol gradient fractions to determine U2 snRNP complexes

The previous experimental results were conflicting. Therefore, we decided to examine glycerol gradient fractions using native gel electrophoresis. We wanted to know if we could distinguish 12S vs. 17S U2 snRNP. We chose the same fractions that were classified to be 12S and 17S U2 snRNP such as in Figure 4-1 (Fractions: 5,6,10,11,12,13,14). Therefore, we looked at U2 snRNA (Figure 4-4 A), core protein SNRPB2 and 15S and 17S U2 snRNP protein SF3B4 (Figure 4-4 B, C). We expect SNRPB2, U2 snRNA and SF3B4 to overlap in the native gel for 17S U2 snRNP and

overlap in U2 snRNA and SNRNPB2 to overlap for 12S U2 snRNP. Proteins and U2 snRNA images were merged in Figure 4-4D. We noticed that in the control nuclear extract proteins and U2 snRNA merged (yellow). We believe that in Figure 4-4D the control lane (N.E.) could possibly be 15S or 17S U2 snRNP.

4.3 Conclusion

We provide a new perspective to study SF3B1 inhibitors in the context of the U2 snRNP. Why we observe a sedimentation difference in U2 RNA in the presence of the drug, but not in proteins. One possibility is that the PB allows for a conformational change in SF3B1 where it allows more formation of 17S U2 snRNP, but another possibility is that the drug is causing aggregations of U2 snRNP. In regard to the native gels, we need to find a method where we can increase the amount of sample that was added. We did not add enough sample and proteins were not able to be detected, and the fractions were thawed and frozen multiple times where it could affect the native state of the complex. In addition, to detecting SF3B4 and SNRNPB2, a protein belonging to the SF3A multi-protein complex should also be studied to confirm or rule out that the merging of the proteins and U2 snRNA in Figure 4-4d is 17S U2 snRNP. Another approach would be to pull-out specific spliceosome complexes and use them as controls to determine complexes in nuclear extract.

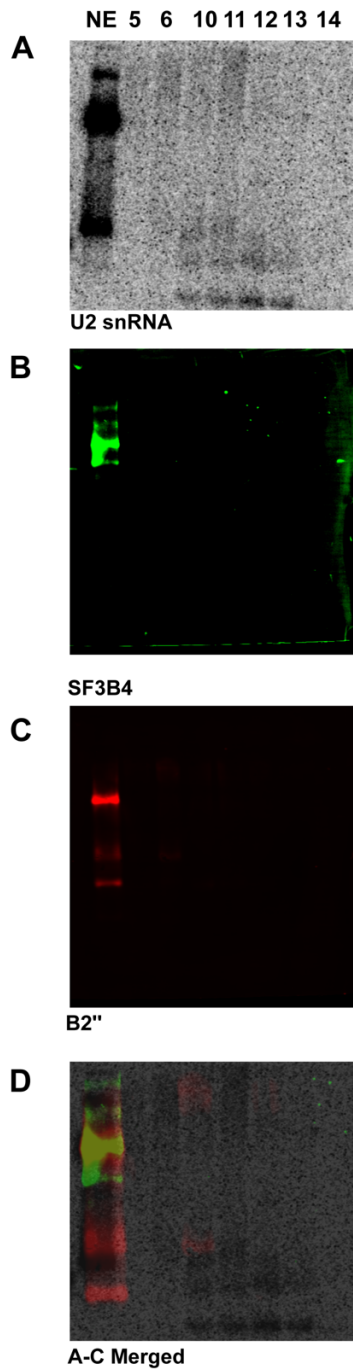


Figure 4-4: Proteins and U2 snRNA in Native Gels. A) Representative Native gel of nuclear extract (N.E.) with fractions 5, 6, 10, 11, 12, 13, 14. U2 snRNA was probed with radiolabeled reversed U2 snRNA oligo. B) NE probed with SF3B4 antibody C) NE probed with SNRPB2 antibody D) Merged images of U2 snRNA, SF3B4 and SNRPB2. Yellow is where SNRPB2 and SF3B3 merge along with U2 snRNA.

4.4 Materials and Methods

Preparing glycerol gradients

Low salt 150mM KCl glycerol gradients were 10-30%. Solutions were made as follows:

Stock (150mM KCl)	Final Concentration	10% (mL)	30% (mL)
KCl (2M)	150 mM	3	3
MgCl ₂ (40mM)	2 mM	2	2
Tris pH 7.9 (200 mM)	20 mM	4	4
Glycerol 50%	10 or 30%	8	24
H ₂ O	-	23	7
Total	-	40	40

Glycerol gradients were poured at room temperature in Seton open-top polyclear centrifuge tubes 9/16x 3.5 inches using syringe with cannula. A total of 6.1mL of the 10% glycerol gradient solution was poured first. Then 6.1mL of the 30% glycerol gradient solution was added by sinking the cannula at the very bottom and released slowly. Glycerol gradients were spun in the 10-30%vw setting for the SW41 rotor and stored in cold room for 30 minutes.

Preparing nuclear extract

Recipe for 150mM KCl	Stock	Final concentration	With PB (μL)	No PB (μL)
Nuclear Extract	80%	31.7%	88	88
tRNA	10 mg/mL	0.1mg/mL	2.2	2.2
MgAc	0.1M	2 mM	4.4	4.4
KCl	2M	150 mM	7.7	7.7
H ₂ O	-	-	117.7	119.9
PB C-3	0.1mM	1 μM	2.2	-
Total	-	-	222.2	222.2

Samples were added in the 30°C water bath for 15 minutes and 200 µL of sample were loaded to glycerol gradients. Run the centrifuge for 29,000 rpm, 18 hours and at 4°C.

Fractionating gradients, denaturing gel preparation and imaging

Glycerol gradients were fractionated manually with 500µL in each tube or using a fractionating piston. RNA was extracted from each sample using phenol pH 4.5: chloroform: Isoamyl . FEB was added to reach RNA pellet and run for 2 hours at 30 Watts in a 12% polyacrylamide and stained with Sybr Gold for RNA. Typhoon scanner was used to image gels.

Native gels

A 20mM Tris/glycine 1.9% low melting agarose was used to make the native gel. For each sample, 20µL of selected glycerol gradient fractions was added along with 2µL of 2x native gel loading dye. We loaded 10µL of sample to each well. For the control nuclear extract, we mixed 4µL of nuclear extract with 2µL of 2x native loading dye. We loaded 2µL to each well. We ran the gel for 3 hours at 72 volts in 20mM Tris/glycine buffer.

Protein Gel

Native gel was transferred to PDVF membrane for 3 hours and 72 volts in Bjerrum Schafer-Nielsen Buffer (Bjerrum and Schafer-Nielsen, 1986). Antibodies against SF3B4 and B2" were used.

Northern blot

Native gel was transferred to a nylon membrane for 20 hours or overnight at 10 volts 30mA and hybridized with the generated U2 snRNA antisense probe by *in vitro* transcription. Native gel protocol to view spliceosome complexes (Konarska and Sharp, 1986)

Bibliography:

Abu Dayyeh, B. K., Quan, T. K., Castro, M., and Ruby, S. W. (2002). Probing interactions between the U2 small nuclear ribonucleoprotein and the DEAD-box protein, Prp5. *J Biol Chem* 277, 20221-20233.

Alsafadi, S., Houy, A., Battistella, A., Popova, T., Wassef, M., Henry, E., Tirode, F., Constantinou, A., Piperno-Neumann, S., Roman-Roman, S., Dutertre, M., and Stern, M. H. (2016). Cancer-associated SF3B1 mutations affect alternative splicing by promoting alternative branchpoint usage. *Nat Commun* 7, 10615.

Arai, K., Buonamici, S., Chan, B., Corson, L., Endo, A., Gerard, B., Hao, M. H., Karr, C., Kira, K., Lee, L., Liu, X., Lowe, J. T., Luo, T., Marcaurelle, L. A., Mizui, Y., Nevalainen, M., O'Shea, M. W., Park, E. S., Perino, S. A., Prajapati, S., Shan, M., Smith, P. G., Tivitmahaisoon, P., Wang, J. Y., Warmuth, M., Wu, K. M., Yu, L., Zhang, H., Zheng, G. Z., and Keaney, G. F. (2014). Total Synthesis of 6-Deoxypladienolide D and Assessment of Splicing Inhibitory Activity in a Mutant SF3B1 Cancer Cell Line. *Org Lett* 16, 5560-5563.

Bai, R., Wan, R., Yan, C., Lei, J., and Shi, Y. (2018). Structures of the fully assembled *Saccharomyces cerevisiae* spliceosome before activation. *Science* 360, 1423-1429.

Behrens, S. E., Tyc, K., Kastner, B., Reichelt, J., and Luhrmann, R. (1993). Small nuclear ribonucleoprotein (RNP) U2 contains numerous additional proteins and has a bipartite RNP structure under splicing conditions. *Mol Cell Biol* 13, 307-319.

Bjerrum, O. J., and Schafer-Nielsen, C. (1986). Buffer systems and transfer parameters for semi-dry electroblotting with horizontal apparatus. *Dunn Electrophoresis* 315-327.

Black, D. L., Chabot, B., and Steitz, J. A. (1985). U2 as well as U1 small nuclear ribonucleoproteins are involved in premessenger RNA splicing. *Cell* 42, 737-750.

Blakemore, D. C., Castro, L., Churcher, I., Rees, D. C., Thomas, A. W., Wilson, D. M., and Wood, A. (2018). Organic synthesis provides opportunities to transform drug discovery. *Nat Chem* 10, 383-394.

Brosi, R., Hauri, H. P., and Kramer, A. (1993). Separation of splicing factor SF3 into two components and purification of SF3a activity. *J Biol Chem* 268, 17640-17646.

Butt, H., Eid, A., Momin, A. A., Bazin, J., Crespi, M., Arold, S. T., and Mahfouz, M. M. (2019). CRISPR directed evolution of the spliceosome for resistance to splicing inhibitors. *Genome Biol* 20, 73.

- Carvalho, T., Martins, S., Rino, J., Marinho, S., and Carmo-Fonseca, M. (2017). Pharmacological inhibition of the spliceosome subunit SF3b triggers exon junction complex-independent nonsense-mediated decay. *J Cell Sci* *130*, 1519-1531.
- Cazzola, M., Rossi, M., Malcovati, L., and Associazione, I. P. L. R. S. C. G. I. M. M. (2013). Biologic and clinical significance of somatic mutations of SF3B1 in myeloid and lymphoid neoplasms. *Blood* *121*, 260-269.
- Chen, S., Anderson, K., and Moore, M. J. (2000). Evidence for a linear search in bimolecular 3' splice site AG selection. *Proc Natl Acad Sci U S A* *97*, 593-598.
- Chiara, M. D., Gozani, O., Bennett, M., Champion-Arnaud, P., Palandjian, L., and Reed, R. (1996). Identification of proteins that interact with exon sequences, splice sites, and the branchpoint sequence during each stage of spliceosome assembly. *Mol Cell Biol* *16*, 3317-3326.
- Corrionero, A., Minana, B., and Valcarcel, J. (2011). Reduced fidelity of branch point recognition and alternative splicing induced by the anti-tumor drug spliceostatin A. *Genes Dev* *25*, 445-459.
- Cretu, C., Agrawal, A. A., Cook, A., Will, C. L., Fekkes, P., Smith, P. G., Luhrmann, R., Larsen, N., Buonamici, S., and Pena, V. (2018). Structural Basis of Splicing Modulation by Antitumor Macrolide Compounds. *Mol Cell* *70*, 265-273 e8.
- Cretu, C., Schmitzova, J., Ponce-Salvatierra, A., Dybkov, O., De Laurentiis, E. I., Sharma, K., Will, C. L., Urlaub, H., Luhrmann, R., and Pena, V. (2016). Molecular architecture of SF3b and structural consequences of its cancer-related mutations. *Mol Cell* *64*, 307-319.
- Darman, R. B., Seiler, M., Agrawal, A. A., Lim, K. H., Peng, S., Aird, D., Bailey, S. L., Bhavsar, E. B., Chan, B., Colla, S., Corson, L., Feala, J., Fekkes, P., Ichikawa, K., Keaney, G. F., Lee, L., Kumar, P., Kunii, K., MacKenzie, C., Matijevic, M., Mizui, Y., Myint, K., Park, E. S., Puyang, X., Selvaraj, A., Thomas, M. P., Tsai, J., Wang, J. Y., Warmuth, M., Yang, H., Zhu, P., Garcia-Manero, G., Furman, R. R., Yu, L., Smith, P. G., and Buonamici, S. (2015). Cancer-Associated SF3B1 Hotspot Mutations Induce Cryptic 3' Splice Site Selection through Use of a Different Branch Point. *Cell Rep* *13*, 1033-1045.
- Dignam, J. D., Lebovitz, R. M., and Roeder, R. D. (1983). Accurate transcription initiation by RNA polymerase II in a soluble extract from isolated mammalian nuclei. *Nucleic Acids Res.* *11*, 1475-1489.
- Effenberger, K. A., Anderson, D. D., Bray, W. M., Prichard, B. E., Ma, N., Adams, M. S., Ghosh, A. K., and Jurica, M. S. (2014). Coherence between cellular responses and

in vitro splicing inhibition for the anti-tumor drug pladienolide B and its analogs. *J Biol Chem* 289, 1938-1947.

Effenberger, K. A., Urabe, V. K., and Jurica, M. S. (2016a). Modulating splicing with small molecular inhibitors of the spliceosome. *Wiley Interdiscip Rev RNA*

Effenberger, K. A., Urabe, V. K., Prichard, B. E., Ghosh, A. K., and Jurica, M. S. (2016b). Interchangeable SF3B1 inhibitors interfere with pre-mRNA splicing at multiple stages. *RNA* 22, 350-359.

Eskens, F. A., Ramos, F. J., Burger, H., O'Brien, J. P., Piera, A., de Jonge, M. J., Mizui, Y., Wiemer, E. A., Carreras, M. J., Baselga, J., and Tabernero, J. (2013). Phase I, Pharmacokinetic and Pharmacodynamic Study of the First-in-Class Spliceosome Inhibitor E7107 in Patients with Advanced Solid Tumors. *Clin Cancer Res*

Finci, L. I., Zhang, X., Huang, X., Zhou, Q., Tsai, J., Teng, T., Agrawal, A., Chan, B., Irwin, S., Karr, C., Cook, A., Zhu, P., Reynolds, D., Smith, P. G., Fekkes, P., Buonamici, S., and Larsen, N. A. (2018). The cryo-EM structure of the SF3b spliceosome complex bound to a splicing modulator reveals a pre-mRNA substrate competitive mechanism of action. *Genes Dev* 32, 309-320.

Folco, E. G., Coil, K. E., and Reed, R. (2011). The anti-tumor drug E7107 reveals an essential role for SF3b in remodeling U2 snRNP to expose the branch point-binding region. *Genes Dev* 25, 440-444.

Furney, S. J., Pedersen, M., Gentien, D., Dumont, A. G., Rapinat, A., Desjardins, L., Turajlic, S., Piperno-Neumann, S., de la Grange, P., Roman-Roman, S., Stern, M. H., and Marais, R. (2013). SF3B1 mutations are associated with alternative splicing in uveal melanoma. *Cancer Discov* 3, 1122-1129.

Ghosh, A. K., and Anderson, D. D. (2012). Enantioselective total synthesis of pladienolide B: a potent spliceosome inhibitor. *Org Lett* 14, 4730-4733.

Ghosh, A. K., and Chen, Z. H. (2013). Enantioselective Syntheses of FR901464 and Spliceostatin A: Potent Inhibitors of Spliceosome. *Org Lett* 15, 5088-5091.

Ghosh, A. K., Chen, Z. H., Effenberger, K. A., and Jurica, M. S. (2014a). Enantioselective Total Syntheses of FR901464 and Spliceostatin A and Evaluation of Splicing Activity of Key Derivatives. *J Org Chem* 79, 5697-5709.

Ghosh, A. K., and Li, J. (2011). A stereoselective synthesis of (+)-herboxidiene/GEX1A. *Org Lett* 13, 66-69.

Ghosh, A. K., Lv, K., Ma, N., Cardenas, E. L., Effenberger, K. A., and Jurica, M. S. (2016). Design, synthesis and in vitro splicing inhibition of desmethyl and carba-derivatives of herboxidiene. *Org Biomol Chem* 14, 5263-5271.

Ghosh, A. K., Ma, N., Effenberger, K. A., and Jurica, M. S. (2014b). Total Synthesis of GEX1Q1, Assignment of C-5 Stereoconfiguration and Evaluation of Spliceosome Inhibitory Activity. *Org Lett* 16, 3154-3157.

Ghosh, A. K., Allu, S. R., Reddy, G. C., Lopez, A. G., Mendez, P., and Jurica, M. S. (2021). Design and synthesis of herboxidiene derivatives that potently inhibit in vitro splicing. *Org Biomol Chem*

Gozani, O., Potashkin, J., and Reed, R. (1998). A potential role for U2AF-SAP 155 interactions in recruiting U2 snRNP to the branch site. *Mol Cell Biol* 18, 4752-4760.

Hepburn, L. A., McHugh, A., Fernandes, K., Boag, G., Proby, C. M., Leigh, I. M., and Saville, M. K. (2018). Targeting the spliceosome for cutaneous squamous cell carcinoma therapy: a role for c-MYC and wild-type p53 in determining the degree of tumour selectivity. *Oncotarget* 9, 23029-23046.

Hong, D. S., Kurzrock, R., Naing, A., Wheler, J. J., Falchook, G. S., Schiffman, J. S., Faulkner, N., Pilat, M. J., O'Brien, J., and Lorusso, P. (2013). A phase I, open-label, single-arm, dose-escalation study of E7107, a precursor messenger ribonucleic acid (pre-mRNA) spliceosome inhibitor administered intravenously on days 1 and 8 every 21 days to patients with solid tumors. *Invest New Drugs*

Hubert, C. G., Bradley, R. K., Ding, Y., Toledo, C. M., Herman, J., Skutt-Kakaria, K., Girard, E. J., Davison, J., Berndt, J., Corrin, P., Hardcastle, J., Basom, R., Delrow, J. J., Webb, T., Pollard, S. M., Lee, J., Olson, J. M., and Paddison, P. J. (2013). Genome-wide RNAi screens in human brain tumor isolates reveal a novel viability requirement for PHF5A. *Genes Dev* 27, 1032-1045.

(2015). *Molecular Oncology Testing for Solid Tumors*.

Kaida, D., Motoyoshi, H., Tashiro, E., Nojima, T., Hagiwara, M., Ishigami, K., Watanabe, H., Kitahara, T., Yoshida, T., Nakajima, H., Tani, T., Horinouchi, S., and Yoshida, M. (2007). Spliceostatin A targets SF3b and inhibits both splicing and nuclear retention of pre-mRNA. *Nat Chem Biol* 3, 576-583.

Kataoka, N. (2017). Modulation of aberrant splicing in human RNA diseases by chemical compounds. *Hum Genet* 136, 1237-1245.

Konarska, M. M., and Sharp, P. A. (1986). Electrophoretic separation of complexes involved in the splicing of precursors to mRNAs. *Cell* 46, 845-55.

- Konarska, M. M., and Sharp, P. A. (1987). Interactions between small nuclear ribonucleoprotein particles in formation of spliceosomes. *Cell* 49, 763-774.
- Kotake, Y., Sagane, K., Owa, T., Mimori-Kiyosue, Y., Shimizu, H., Uesugi, M., Ishihama, Y., Iwata, M., and Mizui, Y. (2007). Splicing factor SF3b as a target of the antitumor natural product pladienolide. *Nat Chem Biol* 3, 570-575.
- Kramer, A., Gruter, P., Groning, K., and Kastner, B. (1999). Combined biochemical and electron microscopic analyses reveal the architecture of the mammalian U2 snRNP. *J Cell Biol* 145, 1355-1368.
- Lagiseti, C., Yermolina, M. V., Sharma, L. K., Palacios, G., Prigaro, B. J., and Webb, T. R. (2014). Pre-mRNA splicing-modulatory pharmacophores: the total synthesis of herboxidiene, a pladienolide-herboxidiene hybrid analog and related derivatives. *ACS Chem Biol* 9, 643-648.
- Larrayoz, M., Blakemore, S. J., Dobson, R. C., Blunt, M. D., Rose-Zerilli, M. J., Walewska, R., Duncombe, A., Oscier, D., Koide, K., Forconi, F., Packham, G., Yoshida, M., Cragg, M. S., Strefford, J. C., and Steele, A. J. (2015). The SF3B1 inhibitor spliceostatin A (SSA) elicits apoptosis in chronic lymphocytic leukaemia cells through downregulation of Mcl-1. *Leukemia*
- Lee, S. C., Dvinge, H., Kim, E., Cho, H., Micol, J. B., Chung, Y. R., Durham, B. H., Yoshimi, A., Kim, Y. J., Thomas, M., Lobry, C., Chen, C. W., Pastore, A., Taylor, J., Wang, X., Krivtsov, A., Armstrong, S. A., Palacino, J., Buonamici, S., Smith, P. G., Bradley, R. K., and Abdel-Wahab, O. (2016). Modulation of splicing catalysis for therapeutic targeting of leukemia with mutations in genes encoding spliceosomal proteins. *Nat Med* 22, 672-678.
- Lin, P. C., and Xu, R. M. (2012). Structure and assembly of the SF3a splicing factor complex of U2 snRNP. *EMBO J* 31, 1579-1590.
- Machida, K., Arisawa, A., Takeda, S., Tsuchida, T., Aritoku, Y., Yoshida, M., and Ikeda, H. (2008). Organization of the biosynthetic gene cluster for the polyketide antitumor macrolide, pladienolide, in *Streptomyces platensis* Mer-11107. *Biosci Biotechnol Biochem* 72, 2946-2952.
- MacMillan, A. M., Query, C. C., Allerson, C. R., Chen, S., Verdine, G. L., and Sharp, P. A. (1994). Dynamic association of proteins with the pre-mRNA branch region. *Genes Dev* 8, 3008-3020.
- MacRae, A. J., Coltri, P., Hrabeta-Robinson, E., Chalkley, R. J., Burlingame, A. L., and Jurica, M. S. (2019). A two-step probing method to compare lysine accessibility across macromolecular complex conformations. *RNA Biol* 1-9.

- Maguire, S. L., Leonidou, A., Wai, P., Marchiò, C., Ng, C. K., Sapino, A., Salomon, A. V., Reis-Filho, J. S., Weigelt, B., and Natrajan, R. C. (2015). SF3B1 mutations constitute a novel therapeutic target in breast cancer. *J Pathol* 235, 571-580.
- Maji, D., Grossfield, A., and Kielkopf, C. L. (2019). Structures of SF3b1 reveal a dynamic Achilles heel of spliceosome assembly: Implications for cancer-associated abnormalities and drug discovery. *Biochim Biophys Acta Gene Regul Mech* 1862, 194440.
- Miller-Wideman, M., Makkar, N., Tran, M., Isaac, B., Biest, N., and Stonard, R. (1992). Herboxidiene, a new herbicidal substance from *Streptomyces chromofuscus* A7847. Taxonomy, fermentation, isolation, physico-chemical and biological properties. *J Antibiot (Tokyo)* 45, 914-921.
- Mizui, Y., Sakai, T., Iwata, M., Uenaka, T., Okamoto, K., Shimizu, H., Yamori, T., Yoshimatsu, K., and Asada, M. (2004). Pladienolides, new substances from culture of *Streptomyces platensis* Mer-11107. III. In vitro and in vivo antitumor activities. *J Antibiot (Tokyo)* 57, 188-196.
- Nakajima, H., Hori, Y., Terano, H., Okuhara, M., Manda, T., Matsumoto, S., and Shimomura, K. (1996a). New antitumor substances, FR901463, FR901464 and FR901465. II. Activities against experimental tumors in mice and mechanism of action. *J Antibiot (Tokyo)* 49, 1204-1211.
- Nakajima, H., SATO, B., FUJITA, T., TAKASE, S., TERANO, H., and, M. O. K. U. H. A. R. A. (1996b). New Antitumor Substances, FR901463, FR901464 and FR901465. I. Taxonomy, Fermentation, Isolation, Physico-chemical Properties and Biological Activities. *Journal of Antibiotics* 49, 1196-1203.
- O'Day, C. L., Dalbadie-McFarland, G., and Abelson, J. (1996). The *Saccharomyces cerevisiae* Prp5 protein has RNA-dependent ATPase activity with specificity for U2 small nuclear RNA. *J Biol Chem* 271, 33261-33267.
- Papaemmanuil, E., Cazzola, M., Boulton, J., Malcovati, L., Vyas, P., Bowen, D., Pellagatti, A., Wainscoat, J. S., Hellstrom-Lindberg, E., Gambacorti-Passerini, C., Godfrey, A. L., Rapado, I., Cvejic, A., Rance, R., McGee, C., Ellis, P., Mudie, L. J., Stephens, P. J., McLaren, S., Massie, C. E., Tarpey, P. S., Varela, I., Nik-Zainal, S., Davies, H. R., Shlien, A., Jones, D., Raine, K., Hinton, J., Butler, A. P., Teague, J. W., Baxter, E. J., Score, J., Galli, A., Della Porta, M. G., Travaglino, E., Groves, M., Tauro, S., Munshi, N. C., Anderson, K. C., El-Naggar, A., Fischer, A., Mustonen, V., Warren, A. J., Cross, N. C., Green, A. R., Futreal, P. A., Stratton, M. R., and Campbell, P. J. (2011). Somatic SF3B1 mutation in myelodysplasia with ring sideroblasts. *N Engl J Med* 365, 1384-1395.

- Parker, R., Siliciano, P. G., and Guthrie, C. (1987). Recognition of the TACTAAC box during mRNA splicing in yeast involves base pairing to the U2-like snRNA. *Cell* *49*, 229-239.
- Plaschka, C., Lin, P. C., Charenton, C., and Nagai, K. (2018). Prespliceosome structure provides insights into spliceosome assembly and regulation. *Nature* *559*, 419-422.
- Plaschka, C., Lin, P. C., and Nagai, K. (2017). Structure of a pre-catalytic spliceosome. *Nature* *546*, 617-621.
- Query, C. C., Strobel, S. A., and Sharp, P. A. (1996). Three recognition events at the branch-site adenine. *EMBO J* *15*, 1392-1402.
- Quesada, V., Conde, L., Villamor, N., Ordonez, G. R., Jares, P., Bassaganyas, L., Ramsay, A. J., Bea, S., Pinyol, M., Martinez-Trillos, A., Lopez-Guerra, M., Colomer, D., Navarro, A., Baumann, T., Aymerich, M., Rozman, M., Delgado, J., Gine, E., Hernandez, J. M., Gonzalez-Diaz, M., Puente, D. A., Velasco, G., Freije, J. M., Tubio, J. M., Royo, R., Gelpi, J. L., Orozco, M., Pisano, D. G., Zamora, J., Vazquez, M., Valencia, A., Himmelbauer, H., Bayes, M., Heath, S., Gut, M., Gut, I., Estivill, X., Lopez-Guillermo, A., Puente, X. S., Campo, E., and Lopez-Otin, C. (2011). Exome sequencing identifies recurrent mutations of the splicing factor SF3B1 gene in chronic lymphocytic leukemia. *Nat Genet* *44*, 47-52.
- Reed, R. (1989). The organization of 3' splice-site sequences in mammalian introns. *Genes Dev* *3*, 2113-2123.
- Rioux, N., Smith, S., Colombo, F., Kim, A., Lai, W. G., Nix, D., Siu, Y. A., Schindler, J., and Smith, P. G. (2020). Metabolic disposition of H3B-8800, an orally available small-molecule splicing modulator, in rats, monkeys, and humans. *Xenobiotica* *50*, 1101-1114.
- Roybal, G. A., and Jurica, M. S. (2010). Spliceostatin A inhibits spliceosome assembly subsequent to prespliceosome formation. *Nucleic Acids Res* *38*, 6664-6672.
- Sakai, T., Sameshima, T., Matsufuji, M., Kawamura, N., Dobashi, K., and Mizui, Y. (2004a). Pladienolides, new substances from culture of *Streptomyces platensis* Mer-11107. I. Taxonomy, fermentation, isolation and screening. *J Antibiot (Tokyo)* *57*, 173-179.
- Sakai, T., Sameshima, T., Matsufuji, M., Kawamura, N., Dobashi, K., and Mizui, Y. (2004b). Pladienolides, new substances from culture of *Streptomyces platensis* Mer-11107. I. Taxonomy, fermentation, isolation and screening. *J Antibiot (Tokyo)* *57*, 173-179.

- Sakai, Y., Tsujita, T., Akiyama, T., Yoshida, T., Mizukami, T., Akinaga, S., Horinouchi, S., Yoshida, M., and Yoshida, T. (2002). GEX1 compounds, novel antitumor antibiotics related to herboxidiene, produced by *Streptomyces* sp. II. The effects on cell cycle progression and gene expression. *J Antibiot (Tokyo)* 55, 863-872.
- Sato, M., Muguruma, N., Nakagawa, T., Okamoto, K., Kimura, T., Kitamura, S., Yano, H., Sannomiya, K., Goji, T., Miyamoto, H., Okahisa, T., Mikasa, H., Wada, S., Iwata, M., and Takayama, T. (2014). High antitumor activity of pladienolide B and its derivative in gastric cancer. *Cancer Sci* 105, 110-116.
- Schmidt, U., Basyuk, E., Robert, M. C., Yoshida, M., Villemin, J. P., Auboeuf, D., Aitken, S., and Bertrand, E. (2011). Real-time imaging of cotranscriptional splicing reveals a kinetic model that reduces noise: implications for alternative splicing regulation. *J Cell Biol* 193, 819-829.
- Seiler, M., Yoshimi, A., Darman, R., Chan, B., Keaney, G., Thomas, M., Agrawal, A. A., Caleb, B., Csibi, A., Sean, E., Fekkes, P., Karr, C., Klimek, V., Lai, G., Lee, L., Kumar, P., Lee, S. C., Liu, X., Mackenzie, C., Meeske, C., Mizui, Y., Padron, E., Park, E., Pazolli, E., Peng, S., Prajapati, S., Taylor, J., Teng, T., Wang, J., Warmuth, M., Yao, H., Yu, L., Zhu, P., Abdel-Wahab, O., Smith, P. G., and Buonamici, S. (2018). H3B-8800, an orally available small-molecule splicing modulator, induces lethality in spliceosome-mutant cancers. *Nat Med* 24, 497-504.
- Smith, C. W., Chu, T. T., and Nadal-Ginard, B. (1993). Scanning and competition between AGs are involved in 3' splice site selection in mammalian introns. *Mol Cell Biol* 13, 4939-4952.
- Smith, C. W., Porro, E. B., Patton, J. G., and Nadal-Ginard, B. (1989). Scanning from an independently specified branch point defines the 3' splice site of mammalian introns. *Nature* 342, 243-247.
- Taggart, A. J., DeSimone, A. M., Shih, J. S., Filloux, M. E., and Fairbrother, W. G. (2012). Large-scale mapping of branchpoints in human pre-mRNA transcripts in vivo. *Nat Struct Mol Biol* 19, 719-721.
- Tang, A. D., Soulette, C. M., van Baren, M. J., Hart, K., Hrabeta-Robinson, E., Wu, C. J., and Brooks, A. N. (2020). Full-length transcript characterization of SF3B1 mutation in chronic lymphocytic leukemia reveals downregulation of retained introns. *Nat Commun* 11, 1438.
- Teng, T., Tsai, J. H., Puyang, X., Seiler, M., Peng, S., Prajapati, S., Aird, D., Buonamici, S., Caleb, B., Chan, B., Corson, L., Feala, J., Fekkes, P., Gerard, B., Karr, C., Korpai, M., Liu, X., J. T. L., Mizui, Y., Palacino, J., Park, E., Smith, P. G., Subramanian, V., Wu, Z. J., Zou, J., Yu, L., Chicas, A., Warmuth, M., Larsen, N., and

- Zhu, P. (2017). Splicing modulators act at the branch point adenosine binding pocket defined by the PHF5A-SF3b complex. *Nat Commun* 8, 15522.
- Thompson, C. F., Jamison, T. F., and Jacobsen, E. N. (2001). FR901464: total synthesis, proof of structure, and evaluation of synthetic analogues. *J Am Chem Soc* 123, 9974-9983.
- van der Feltz, C., and Hoskins, A. A. (2019). Structural and functional modularity of the U2 snRNP in pre-mRNA splicing. *Crit Rev Biochem Mol Biol* 54, 443-465.
- Vigevani, L., Gohr, A., Webb, T., Irimia, M., and Valcarcel, J. (2017). Molecular basis of differential 3' splice site sensitivity to anti-tumor drugs targeting U2 snRNP. *Nat Commun* 8, 2100.
- Wilkinson, M. E., Charenton, C., and Nagai, K. (2020). RNA Splicing by the Spliceosome. *Annu Rev Biochem* 89, 359-388.
- Will, C. L., Schneider, C., MacMillan, A. M., Katopodis, N. F., Neubauer, G., Wilm, M., Luhrmann, R., and Query, C. C. (2001). A novel U2 and U11/U12 snRNP protein that associates with the pre-mRNA branch site. *EMBO J* 20, 4536-4546.
- Will, C. L., Urlaub, H., Achsel, T., Gentzel, M., Wilm, M., and Luhrmann, R. (2002). Characterization of novel SF3b and 17S U2 snRNP proteins, including a human Prp5p homologue and an SF3b DEAD-box protein. *EMBO J* 21, 4978-4988.
- Wu, G., Fan, L., Edmonson, M. N., Shaw, T., Boggs, K., Easton, J., Rusch, M. C., Webb, T. R., Zhang, J., and Potter, P. M. (2018). Inhibition of SF3B1 by molecules targeting the spliceosome results in massive aberrant exon skipping. *RNA* 24, 1056-1066.
- Wu, J., and Manley, J. L. (1989). Mammalian pre-mRNA branch site selection by U2 snRNP involves base pairing. *Genes Dev* 3, 1553-1561.
- Yan, C., Wan, R., Bai, R., Huang, G., and Shi, Y. (2016). Structure of a yeast activated spliceosome at 3.5 Å resolution. *Science* 353, 904-911.
- Yokoi, A., Kotake, Y., Takahashi, K., Kadowaki, T., Matsumoto, Y., Minoshima, Y., Sugi, N. H., Sagane, K., Hamaguchi, M., Iwata, M., and Mizui, Y. (2011). Biological validation that SF3b is a target of the antitumor macrolide pladienolide. *FEBS J* 278, 4870-4880.
- Yoshida, K., and Ogawa, S. (2014). Splicing factor mutations and cancer. *Wiley Interdiscip Rev RNA* 5, 445-459.

Yoshida, K., Sanada, M., Shiraishi, Y., Nowak, D., Nagata, Y., Yamamoto, R., Sato, Y., Sato-Otsubo, A., Kon, A., Nagasaki, M., Chalkidis, G., Suzuki, Y., Shiosaka, M., Kawahata, R., Yamaguchi, T., Otsu, M., Obara, N., Sakata-Yanagimoto, M., Ishiyama, K., Mori, H., Nolte, F., Hofmann, W. K., Miyawaki, S., Sugano, S., Haferlach, C., Koeffler, H. P., Shih, L. Y., Haferlach, T., Chiba, S., Nakauchi, H., Miyano, S., and Ogawa, S. (2011). Frequent pathway mutations of splicing machinery in myelodysplasia. *Nature* 478, 64-69.

Yoshikawa, Y., Ishibashi, A., Takehara, T., Suzuki, T., Murai, K., Kaneda, Y., Nimura, K., and Arisawa, M. (2020). Design and Synthesis of 1,2-Deoxy-pyranose Derivatives of Spliceostatin A toward Prostate Cancer Treatment. *ACS Med Chem Lett* 11, 1310-1315.

Yoshimoto, R., Kaida, D., Furuno, M., Burroughs, A. M., Noma, S., Suzuki, H., Kawamura, Y., Hayashizaki, Y., Mayeda, A., and Yoshida, M. (2017). Global analysis of pre-mRNA subcellular localization following splicing inhibition by spliceostatin A. *RNA* 23, 47-57.

Zhang, Q., Di, C., Yan, J., Wang, F., Qu, T., Wang, Y., Chen, Y., Zhang, X., Liu, Y., Yang, H., and Zhang, H. (2019). Inhibition of SF3b1 by pladienolide B evokes cycle arrest, apoptosis induction and p73 splicing in human cervical carcinoma cells. *Artif Cells Nanomed Biotechnol* 47, 1273-1280.

Zhang, Z., Will, C. L., Bertram, K., Dybkov, O., Hartmuth, K., Agafonov, D. E., Hofele, R., Urlaub, H., Kastner, B., Lührmann, R., and Stark, H. (2020). Molecular architecture of the human 17S U2 snRNP. *Nature* 583, 310-313.

Zhou, Z., Gong, Q., Wang, Y., Li, M., Wang, L., Ding, H., and Li, P. (2020). The biological function and clinical significance of SF3B1 mutations in cancer. *Biomark Res* 8, 38.

Zhuang, Y., and Weiner, A. M. (1989). A compensatory base change in human U2 snRNA can suppress a branch site mutation. *Genes Dev* 3, 1545-1552.